


Dispersive Readout of Molecular Spin Qudits

Álvaro Gómez-León^{1,*}, Fernando Luis², and David Zueco²

¹*Instituto de Física Fundamental IFF-CSIC, Calle Serrano 113b, Madrid 28006, Spain*

²*Instituto de Nanociencia y Materiales de Aragón (INMA), CSIC-Universidad de Zaragoza, Zaragoza 50009, Spain*

 (Received 8 October 2021; revised 4 March 2022; accepted 13 May 2022; published 14 June 2022)

We study the physics of a magnetic molecule described by a “giant” spin with multiple ($d > 2$) spin states interacting with the quantized cavity field produced by a superconducting resonator. By means of the input-output formalism, we derive an expression for the output modes in the dispersive regime of operation. It includes the effect of magnetic anisotropy, which makes different spin transitions addressable. We find that the measurement of the cavity transmission allows us to uniquely determine the spin state of the qudits. We discuss, from an effective Hamiltonian perspective, the conditions under which the qudit readout is a nondemolition measurement and consider possible experimental protocols to perform it. Finally, we illustrate our results with simulations performed for realistic models of existing magnetic molecules.

DOI: [10.1103/PhysRevApplied.17.064030](https://doi.org/10.1103/PhysRevApplied.17.064030)

I. INTRODUCTION

Circuit quantum electrodynamics (QED) studies the coupling of quantized cavity modes in superconducting resonators to “artificial atoms” [1,2]. It provides a practical method to readout the state of circuits involving Josephson junctions [3]. The readout protocol is based on measuring the shift of the cavity resonance frequency induced by its coupling to the qubit. When the two systems are energetically detuned from each other, a condition often referred to as the dispersive regime, the shift depends on whether the latter is in state “0” or “1” [4]. This technology has been applied in most of the currently available quantum processors that use superconducting qubits [5,6].

In the last decade, circuit QED has been enriched with studies of hybrid platforms, in which electron [7] and, particularly, spin ensembles [8,9] are coupled to on-chip superconducting cavities. Different magnetic species have already been studied in this context, including impurity spins in semiconductors [10–13], lanthanide ions [14,15], and magnetic molecules [16–19]. A potential application of these schemes is the implementation of quantum memories [20], exploiting the fact that some spin systems exhibit very long coherence times [21]. Yet, spins can also perform as operational qubits [22]. Hybrid processors based on microscopic spins coupled to, and through, on-chip resonators could outperform superconducting processors on account of their larger potential for integrating many resources in a single device [23–25].

In connection with the latter idea, a further appealing property of solid state spins is that they provide natural realizations of qudits, i.e., quantum systems with $d > 2$ discrete levels. The ability to use additional states provides resources for quantum information processing [26,27], which can be especially useful for the implementation of specific quantum error correction codes [28–30] or the quantum simulation of problems involving multiple degrees of freedom [31]. Of particular relevance in this context are artificial magnetic molecules [32,33] (see Fig. 1), whose composition and structure can be chemically tuned to create well-defined systems with multiple and experimentally accessible low-lying spin states [34–41]. The challenge is finding practical methods to operate these multidimensional quantum spin systems.

In this work, we study the possibility of reading out the states of molecular spin qudits via their coupling to cavity photons (see Fig. 1). Our main goal is to generalize the dispersive readout protocol known for qubits to the case of qudits. However, this generalization is not straightforward. Magnetic molecules require some careful considerations, on account of their inherent level multiplicity, the presence of a complex ligand field, and, in the case of molecules hosting more than a single magnetic ion, spin-spin interactions. The last two contributions make the different levels unequally spaced, thus allowing one to spectroscopically address each resonant transition. Yet, they also introduce some marked quantitative and qualitative differences with respect to the case of qubits. These aspects determine how the readout process modifies the qudit state and open diverse alternatives for its experimental implementation.

*a.gomez.leon@csic.es

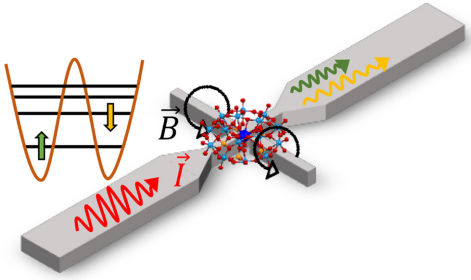


FIG. 1. Schematic setup where a magnetic molecule is placed on a constriction fabricated in the central line of a superconducting coplanar resonator. Sending microwave pulses and detecting transmission allows us to differentiate between the multiple molecular spin states due to the different frequency shifts they generate on the cavity frequency.

Last but not least, since first realizations will likely involve experiments on molecular crystals, in order to enhance the collective spin-photon couplings, one needs to also consider the inhomogeneous broadening of the spin qubit levels.

In order to rigorously address these questions, we calculate the transmission of a cavity coupled to one or several spin qubits using the input-output formalism [42–44]. Then, we obtain analytical expressions for the (state-dependent) cavity frequency shift in the dispersive regime. Furthermore, using a Schrieffer-Wolff transformation, we derive an effective Hamiltonian for the dressed spin states, which describes the spin-photon coupled system. This allows us to address the nondemolition nature of the spin state readout [45]. The general theory is tested in four examples. First, we study a simple $S = 1$ spin model with purely uniaxial anisotropy, which closely resembles the physics of nitrogen-vacancy centers. Then, we move on to molecules that illustrate three different prototypical situations: a GdW_{30} qubit [37] based on a large $S = 7/2$ electronic spin, the $[\text{CeEr}]$ molecular dimer [35], which hosts two weakly interacting effective spin-1/2 systems, and the ^{173}Yb -trensal, which couples an effective $S = 1/2$ electronic spin to an $I = 5/2$ nuclear spin. The remainder of the manuscript is organized as follows. Section II is devoted to the general theory for the coupling of molecular magnets and superconducting cavities or LC resonators, the dispersive readout formulas, and the nondemolition character of the measurement. Then, Sec. III reports the different examples where we apply the theory discussing the feasibility of our proposal. We close the paper with some conclusions. Technical details and concepts of minor importance are deferred to the appendices.

II. THEORY

A. Magnetic circuit QED

Most molecular magnets are both neutral and exhibit a close to zero electric dipole. In many cases, they are

accurately described by a simple “giant” spin- S effective Hamiltonian \mathcal{H}_S , which includes the effects of magnetic anisotropy and the couplings to magnetic fields [46,47]. This Hamiltonian is naturally written in terms of Stevens operators:

$$\mathcal{H}_S = \sum_{k=2,4,6} \sum_{q=-k}^k B_k^q \hat{O}_k^q(\vec{S}) + \mu_B \vec{B} \cdot \hat{g} \cdot \vec{S}. \quad (1)$$

Here the B_k^q are magnetic anisotropy constants, $\vec{S} = (S^x, S^y, S^z)$ are spin operators with $[S^j, S^k] = i\epsilon_{jkl}S^l$, μ_B is the Bohr magneton, $\vec{B} = (b_x, b_y, b_z)$ is the external magnetic field, and \hat{g} is the gyromagnetic tensor. Because of the anisotropy terms in Eq. (1), the molecule is characterized by a set of $2S + 1$ unequally spaced energy levels that can be independently addressed and used to define a qudit [25,37,40,41,48–50]. For simplicity, we use Eq. (1) to define our qudit and to illustrate the theory describing the coupling to cavity photons. The same formalism can be adapted to more complex situations that fall beyond the giant spin approximation. The case of two weakly coupled spins is considered below for the molecular lanthanide dimer $[\text{CeEr}]$, as well as the case of ^{173}Yb -trensal, which contains electronuclear spin states involving the electronic and nuclear spins.

The coupling of molecular magnets to a superconducting cavity or LC resonator is described by the generalized Dicke model, which reduces to the quantum Rabi model for the case of a single molecule [23,51]. This description can be further simplified to a Jaynes-Cummings model, by neglecting counter-rotating terms. However, as we are interested in the dispersive regime, which avoids resonances, and the role of counter-rotating terms can be relevant to some extent, we keep them and use the more general description of the system. The electromagnetic field in the cavity or LC resonator is quantized and its Hamiltonian is given by

$$\mathcal{H}_c = \Omega a^\dagger a \quad (2)$$

with Ω its frequency and a (a^\dagger) the photonic annihilation (creation) operators that fulfil $[a, a^\dagger] = 1$. The local quantized magnetic field generated by the superconducting currents can be written as $\vec{B}_{\text{mw}}(\vec{r}) = \vec{B}_{\text{rms}}(\vec{r})(a^\dagger + a)$ with $\vec{B}_{\text{rms}}^2(\vec{r}) = \langle 0 | \vec{B}_{\text{mw}}^2(\vec{r}) | 0 \rangle$ its zero-point fluctuations. This quantum field couples to the spin via the Zeeman interaction and therefore adds a contribution analogous to the second term in Eq. (1), with the difference that in this case there will be back reaction between the spin and photon fields. Therefore, the total Hamiltonian is

$$\mathcal{H} = \mathcal{H}_S + \mathcal{H}_I + \mathcal{H}_c \quad (3)$$

with

$$\mathcal{H}_I = (a^\dagger + a)\vec{\lambda} \cdot \hat{g} \cdot \vec{S} \quad (4)$$

and $\vec{\lambda} = \mu_B \vec{B}_{\text{rms}}(\vec{r})$ the coupling constant for a molecule at position \mathbf{r} . The specific form of \mathcal{H}_I will slightly change for the cases of the [CeEr] dimer and the ^{173}Yb -trensral electronuclear molecule. However, its treatment is analogous in all cases.

B. Dispersive readout and state-dependent cavity transmission

Dispersive readout was developed for the nondemolition readout of qubits. The main idea is to obtain information of a quantum system indirectly, by measuring its effect on the propagation of the cavity photons. In the dispersive regime, where the qubit is detuned from the cavity, the state of the former shows a one-to-one correspondence with the frequency shift of the latter, which can be determined by measuring the transmission through the device [4,52]. Importantly, this readout is a nondemolition measurement [53,54], which greatly improves the potential use of this technique. The generalization of the readout protocol to qudits in magnetic molecules is not straightforward. The two main difficulties lie in the multilevel energy spectrum for spin $S > 1/2$ [55] and in the presence of magnetic nonlinear contributions from the anisotropy terms. We show now how to perform this generalization.

For simplicity, we first focus on the case of a single molecule interacting with the cavity field, but its generalization to an ensemble of molecules is also addressed below. For our purposes, it is convenient to write the spin operators in Eq. (3) in the basis of eigenstates of \mathcal{H}_S . In this basis, the Hamiltonian for the magnetic molecule takes the very simple form

$$\mathcal{H}_S = \sum_{\alpha=1}^{2S+1} E_\alpha X^{\alpha,\alpha}, \quad (5)$$

where $X^{\alpha,\alpha} = |\alpha\rangle\langle\alpha|$ is the projector onto the eigenstate $|\alpha\rangle$, with energy E_α . Similarly, the interaction Hamiltonian \mathcal{H}_I in Eq. (4) takes the form

$$\mathcal{H}_I = (a^\dagger + a) \sum_{\bar{\alpha}=1}^{2S+1} \Lambda_{\bar{\alpha}} X^{\bar{\alpha}}, \quad (6)$$

where $X^{\bar{\alpha}} = |\alpha_1\rangle\langle\alpha_2|$ are Hubbard operators [56]. The matrix $\Lambda_{\bar{\alpha}}$ can be explicitly written in terms of the S^z eigenstates $|S, M\rangle$. However, to write its explicit form below, we consider that the gyromagnetic tensor \hat{g} is diagonal, with nonzero elements (g_x, g_y, g_z) . This assumption is not strictly necessary, but it is always possible for single-ion magnets and highly reduces the number of terms.

For molecules with several ions within the same cluster, special care is required, but we discuss below how to deal with them using the example of the molecular complex [CeEr]. After some algebra, $\Lambda_{\bar{\alpha}}$ reads

$$\begin{aligned} \Lambda_{\bar{\alpha}} = & \lambda_z g_z \sum_{M=-S}^S M c_{\alpha_1, M} c_{\alpha_2, M}^* \\ & + \sum_{M=-S}^S \gamma_{S, M} \frac{\lambda_x g_x - i\lambda_y g_y}{2} c_{\alpha_1, M+1} c_{\alpha_2, M}^* \\ & + \sum_{M=-S}^S \gamma_{S, M} \frac{\lambda_x g_x + i\lambda_y g_y}{2} c_{\alpha_1, M} c_{\alpha_2, M+1}^* \end{aligned} \quad (7)$$

with $\gamma_{S, M} = \sqrt{S(S+1) - M(M+1)}$ and $c_{\alpha, M} = \langle\alpha|M, S\rangle$. The advantage of working with Hubbard operators is that the nonlinear contributions from the anisotropy terms are nicely encoded in the eigenstates $|\alpha\rangle$. Now we discuss how to link the spectral features of the molecule with the cavity photons.

To explore the cavity transmission in a two-port setup (see the schematic in Fig. 1), we consider the input-output formalism [57]. Following the general theory, the cavity field is computed using a quantum Langevin-like equation where the input field is explicitly considered as a source:

$$\partial_t a = -i\left(\Omega - i\frac{\gamma}{2}\right)a - i \sum_{\bar{\alpha}=1}^{2S+1} \Lambda_{\bar{\alpha}} X^{\bar{\alpha}} - \sum_{l=1,2} \sqrt{\gamma_l} b_{\text{in}, l}. \quad (8)$$

Equation (8) describes the time evolution of a photon operator in a cavity with frequency Ω and total cavity loss $\gamma = \gamma_1 + \gamma_2$ ($\gamma = \Omega/Q$, with Q the quality factor). Here, γ is expected to be small, in order to describe the Markovian environment produced by the resonator loses, and for the system to work in the dispersive regime. In addition, $b_{\text{in}, l}$ is the input signal sent to the cavity or LC resonator through a transmission line at port l .

To solve the equation of motion for the photon operator, one needs to apply a truncation scheme, to find a solution for $X^{\bar{\alpha}}$. Otherwise, the equation of motion for a couples to the equation of motion for $X^{\bar{\alpha}}$, which couples to many-body operators of the form $aX^{\bar{\alpha}}$ and $a^\dagger X^{\bar{\alpha}}$, and so on. A natural choice for experiments is to consider that the interaction between a single spin and the cavity photons is small. In that case, when both subsystems are coupled, they remain almost unaltered and the corrections can be expressed in power series of $\Lambda_{\bar{\alpha}}$. Therefore, in this case the Heisenberg equation of motion for a generic Hubbard operator can be simplified to

$$\dot{X}^{\bar{\alpha}} \simeq iE_{\bar{\alpha}} X^{\bar{\alpha}} + i(a + a^\dagger) \Lambda_{\alpha_2, \alpha_1} (\langle X^{\alpha_2, \alpha_2} \rangle - \langle X^{\alpha_1, \alpha_1} \rangle) \quad (9)$$

with $E_{\bar{\alpha}} = E_{\alpha_1} - E_{\alpha_2}$ the energy difference. To obtain Eq. (9), we have neglected terms of order two or higher

in $\Lambda_{\bar{\alpha}}$. This makes the off-diagonal averages $\langle a^\dagger \rangle$, $\langle a \rangle$, and $\langle X^{\alpha,\beta} \rangle$ (for $\alpha \neq \beta$) to approximately vanish. Now Eqs. (8) and (9) form a closed set that can be easily solved with a Fourier transform to the frequency domain. Importantly, note that Eq. (9) is valid for arbitrary dissipation, which means that the solution can be used to explore both the weak- and strong-coupling regimes [58,59].

Finally, in order to obtain more compact expressions, we consider that the molecules can be described by a density matrix that is diagonal in the basis of eigenstates $\rho = \sum_{\alpha=1}^{2S+1} p_\alpha X^{\alpha,\alpha}$. This is compatible with the weak coupling assumption and realistic in experiments due to the initial state preparation. Finally, as the transmission is defined as $t_c = \langle b_{\text{out},2} \rangle / \langle b_{\text{in},1} \rangle$, we find from the input-output relations that

$$t_c(\omega) = \frac{i\sqrt{\gamma_1\gamma_2}}{\Omega - \omega - i\gamma/2 + \sum_{\bar{\alpha}} p_{\bar{\alpha}} |\Lambda_{\bar{\alpha}}|^2 / (\omega + E_{\bar{\alpha}} + i\eta)}, \quad (10)$$

where we have assumed that the input field enters via port 1. Here, η is the phenomenological broadening of the molecular spin levels and we have defined $|\Lambda_{\bar{\alpha}}|^2 \equiv \Lambda_{\alpha_1,\alpha_2} \Lambda_{\alpha_2,\alpha_1}$ and $p_{\bar{\alpha}} \equiv p_{\alpha_1} - p_{\alpha_2}$. Equation (10) shows that the transmission depends on the state of the molecular spin and generalizes the dispersive readout of qubits to qudits with nonlinear terms. Furthermore, we can extract from Eq. (10) the photon frequency shift measured at $\omega \sim \Omega$ for a molecule in state β and with small spectral broadening η , which is given by

$$\delta\tilde{\Omega}_\beta = 2 \sum_{\alpha=1}^{2S+1} \frac{|\Lambda_{\alpha,\beta}|^2 E_{\alpha,\beta}}{\Omega^2 - E_{\alpha,\beta}^2}. \quad (11)$$

The theory presented so far applies to single molecules. However, in experimental setups it is common to consider crystals, and thus ensembles of molecules. This is useful because the effective coupling and the signal it generates is enhanced with the number of molecules N that couple to the quantized field. In this case, Eq. (10) is still valid, but the frequency shift acquires an enhancement proportional to N :

$$\delta\tilde{\Omega}_\beta(\omega) = \sum_{i=1}^N \sum_{\alpha=1}^{2S+1} \frac{2|\Lambda_i^{\alpha,\beta}|^2 E_{\alpha,\beta}}{(\omega + i\eta)^2 - E_{\alpha,\beta}^2} \quad (12)$$

with $\Lambda_i^{\alpha,\beta}$ the matrix elements for each molecule. The detailed derivation for the case of inhomogeneous couplings and the discussion about the regime of validity are given in Appendix A.

C. Quantum nondemolition character

As previously stated, one of the advantages of the dispersive readout is the quantum nondemolition (QND)

nature of the measurement. This property can be easily understood in the qubit case from the effective Hamiltonian, to second order in the interaction, obtained using a Schrieffer-Wolff transformation [60]. There, the qubit and the photon frequency correction terms commute, indicating that a projective measurement of the photon frequency will not change the qubit state. This result does not necessarily hold in the case of a qudit, especially due to the presence of magnetic anisotropy terms. We now derive an effective Hamiltonian to second order in $\Lambda_{\bar{\alpha}}$ to check if the dispersive readout is still a QND measurement for magnetic molecules.

The Schrieffer-Wolff transformation is defined in terms of a matrix \mathcal{S} [60]:

$$\tilde{\mathcal{H}} = e^{\mathcal{S}} \mathcal{H} e^{-\mathcal{S}} = \mathcal{H}_0 + \frac{1}{2}[\mathcal{S}, \mathcal{H}_I] + \mathcal{O}(\Gamma^3). \quad (13)$$

Here $\mathcal{H}_0 = \mathcal{H}_S + \mathcal{H}_c$, Γ is a small parameter (see below), and we have imposed $[\mathcal{H}_0, \mathcal{S}] = \mathcal{H}_I$ in Eq. (13) to push the coupling term to second order. This last condition is met with the ansatz

$$\mathcal{S} = \sum_{\bar{\beta}=1}^{2S+1} (\Gamma_{+}^{\bar{\beta}} a^\dagger + \Gamma_{-}^{\bar{\beta}} a) X^{\bar{\beta}}, \quad \Gamma_{\pm}^{\bar{\beta}} = \frac{\Lambda_{\bar{\beta}}}{E_{\bar{\beta}} \pm \Omega}. \quad (14)$$

Note that it has been possible to find this ansatz due to the use of Hubbard operators. Otherwise, the nonlinear terms from the magnetic anisotropy would spoil its derivation. After some algebra and the same approximations used to derive the cavity transmission $t_c(\omega)$, we find that (see Appendix C for a detailed derivation)

$$\begin{aligned} \tilde{\mathcal{H}} \simeq & \sum_{\alpha=1}^{2S+1} E_\alpha X^{\alpha,\alpha} + \Omega a^\dagger a \\ & + \sum_{\alpha,\beta=1}^{2S+1} \frac{|\Lambda_{\alpha,\beta}|^2}{E_{\alpha,\beta} - \Omega} \left(1 + a^\dagger a \frac{2E_{\alpha,\beta}}{E_{\alpha,\beta} + \Omega} \right) X^{\alpha,\alpha}. \end{aligned} \quad (15)$$

Equation (15) is derived under the assumption of small interaction, with respect to the qudit levels detuning from the cavity (i.e., $\Lambda_{\bar{\beta}} < ||E_{\bar{\beta}} - \Omega||$), and is valid to describe the weak- and strong-coupling regimes [58]. Also, Eq. (15) perfectly agrees with the cavity frequency shift predicted for the qudit state β in Eq. (11). Finally, the effective Hamiltonian also encodes some extra information, such as the effect of magnetic anisotropy in the effective spin-photon interaction and the energy shift of each individual qudit level.

To check the QND nature of the readout, we calculate the commutator between the molecule Hamiltonian \mathcal{H}_S and the frequency shift term in the effective Hamiltonian, which we denote as $\tilde{\mathcal{V}}$. As the effective Hamiltonian in Eq. (15) is obtained by keeping diagonal terms only, both

terms commute and we could conclude that the readout is a nondemolition measurement. This is true for sufficiently short timescales, where diagonal contributions dominate. However, the off-diagonal terms, previously discarded to obtain Eq. (15), can become relevant at longer times if, e.g., the measurement protocol is relatively slow. If these terms are kept, we find that, in general,

$$[\mathcal{H}_S, \tilde{\mathcal{V}}] = \sum_{\beta_i=1}^{2S+1} E_{\tilde{\beta}} \Phi_{\tilde{\beta}} X^{\tilde{\beta}}, \quad (16)$$

where $\Phi_{\tilde{\beta}}$ is a scalar function of the state β (see Appendix C for details). This breakdown of the QND measurement can happen even for a qubit, if the interaction with the photon field is not completely orthogonal to the qubit quantization axis. However, the qudit case introduces some additional ingredients. As we show below for the specific case of a molecule with $S = 1$, even for a perfectly orthogonal photon field, the crystal anisotropy introduces a nonvanishing correction. Nevertheless, even in this case it is possible to cancel this effect by applying suitably aligned dc magnetic fields.

III. RESULTS AND DISCUSSION

Our results reproduce the well-known expressions for the qubit case ($S = 1/2$) [52] and the effective Hamiltonian is explicitly obtained in Appendix B. In what follows, we discuss three relevant examples to explore the performance of our proposal for the state-dependent readout of molecular qudits.

A. Toy model ($S = 1$)

Probably the simplest generalization to qubits ($S = 1/2$) is the case of a qutrit ($S = 1$) with uniaxial anisotropy, a magnetic field aligned with the anisotropy axis, and a purely transverse coupling $\tilde{\lambda} = (\lambda_x, 0, 0)$ [cf. Eqs. (1), (3), and (6)]:

$$\mathcal{H} = D(S^z)^2 + \xi_z S^z + \Omega a^\dagger a + \lambda_x g_x (a^\dagger + a) S^x. \quad (17)$$

Here, D is the second-order magnetic anisotropy constant and $\xi_z = g_z \mu_B B_z$. A key advantage of this model is that the eigenvectors of \mathcal{H}_S are spanned by the S^z basis. The energies are $E_{\pm} = D \pm \xi_z$ and $E_0 = 0$, while $\Lambda_{\tilde{M}} = \lambda_x g_x / \sqrt{2}$ for $M_1 - M_2 = \pm 1$, and zero otherwise. As a consequence, in this case the photon frequency shifts can be analytically obtained as

$$\delta \tilde{\Omega}_{\pm} = \frac{\lambda_x^2 g_x^2 E_{\pm}}{E_{\pm}^2 - \Omega^2}, \quad (18)$$

$$\delta \tilde{\Omega}_0 = -\lambda_x^2 g_x^2 \left(\frac{E_+}{E_+^2 - \Omega^2} + \frac{E_-}{E_-^2 - \Omega^2} \right), \quad (19)$$

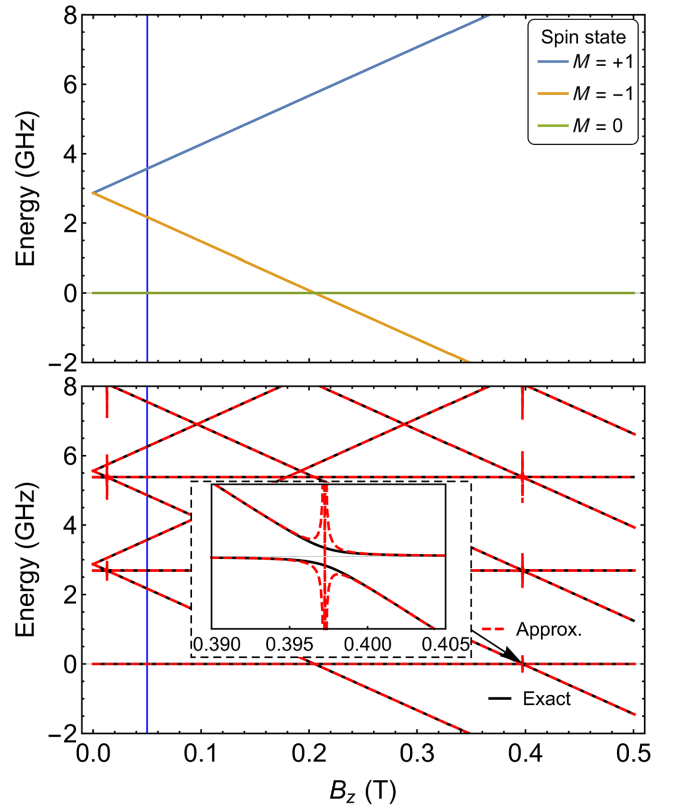


FIG. 2. Top: energy levels for an isolated $S = 1$ molecule (N-V center) with a purely uniaxial anisotropy. Bottom: energy levels for the spin-cavity system with resonator frequency $\Omega \simeq 2.69$ GHz. The spectrum (solid black line) from exact diagonalization of Hamiltonian (17) is compared to the approximation using Eq. (15) (red dashed line). The inset shows an enlarged view of the region where the system is not in the dispersive regime due to a resonance between the qutrits and cavity.

and, importantly, as the shifts are state dependent, in theory the molecular spin states could be resolved spectroscopically.

Nitrogen-vacancy (N-V) centers [61] in diamond provide an interesting physical realization of an $S = 1$ system that can be accurately described by this simple model. The three lowest-energy states can be described with a magnetic anisotropy parameter $D \simeq 2.87$ GHz. This is shown in Fig. 2 (top), where we plot the energy levels of an isolated N-V center as a function of the longitudinal field B_z .

In this system, each single N-V center weakly couples to photons. However, the strong-coupling regime has been achieved for the ensemble of N-V centers in diamond crystals [62], with collective coupling strengths in the megahertz range. Here, we take the experimental parameters reported in Ref. [62], in order to check the feasibility of the readout in a realistic setup. To find a range of parameters in which the spin-cavity system lies in the dispersive regime, in Fig. 2 (bottom) we compare the exact

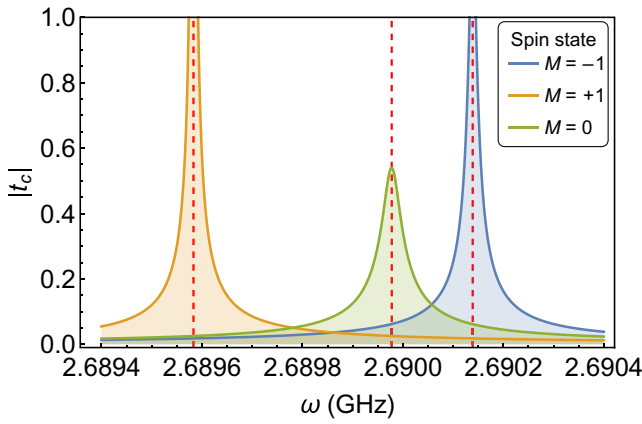


FIG. 3. Plot of $|t_c|$ versus ω for different states of an ensemble of $S = 1$ qudits or N-V centers ($d = 3$) and $\gamma_j = 4 \times 10^{-5}$ GHz. The inset shows the transmission phase ϕ . Vertical dashed lines indicate the predicted frequency shift from Eq. (11). The difference in amplitude between peaks is produced by the dissipative terms and the detuning of each transition from Ω .

spectrum of Eq. (17) with the effective Hamiltonian from Eq. (15) for a collective coupling in the megahertz range. The plot shows very good agreement between the two, with the exception of regions where spins and cavity are resonant, as shown in the enlarged area near a resonant anticrossing. The vertical blue line indicates our choice of the magnetic field to perform the readout.

In experiments with N-V centers [62], the resonator frequencies are close to D . Here, we take $\Omega = 2.6899$ GHz and the inhomogeneous spin broadening $\eta \simeq 9.4$ MHz. When the strong-coupling regime is attained, the estimated value of the collective coupling results in $g_x \lambda_x \sqrt{N} \simeq 19.2$ MHz. With these values, we can discuss the readout of the qutrit state in ensembles of N-V centers.

Figure 3 shows the transmission amplitude as a function of frequency for the different spin states of an $S = 1$ molecule or a N-V center. The static longitudinal field is marked with a vertical blue line in Fig. 2, where the dispersive regime is well justified. As a further numerical check, we have confirmed that the positions of the peaks in Fig. 3 agree with the peaks from the spectral function, calculated with exact diagonalization. The inset shows the transmission phase, which also depends on the spin state. Phase acquisition has the advantage of having less fluctuations, so it can be measured more accurately. It also provides a quite direct method to determine the qudit spin state by measuring its sign on both sides of the central frequency and applying the truth table $++ \rightarrow M = -1$, $+ - \rightarrow M = +1$, and $-- \rightarrow M = 0$.

Importantly, for illustrative purposes, we have considered in Fig. 3 a resonator with losses $\gamma_j \simeq 10^{-5}$ GHz. This value is smaller than that considered in Ref. [62], but it is still realistic. The reason is that, for larger losses, the peaks in Fig. 3 broaden and overlap; however, this does not mean

that the state cannot be detected, as the phase measurement remains almost unchanged. This means that the qudit readout is not highly constrained by the spin broadening (which is much larger in this case) and that phase measurements are robust, even for realistic resonators and in the presence of a sizeable inhomogeneous broadening.

This example demonstrates that the dispersive readout of an ensemble of molecules or other spin systems with $S > 1/2$ and magnetic anisotropy is feasible. However, an important difference is that the characterization of the spin qudit state requires one to perform $d - 1$ measurements. Nevertheless, this could be experimentally mitigated by considering multifrequency pulses such as frequency combs that have been applied to multiplex the readout of arrays of LC resonators used as radiation detectors in astronomy [63]. The pulse design can be likely optimized via the application of optimal control techniques, just as is done with spin control pulses [64].

As we discussed in Sec. II C, another difference with respect to qudits is the QND character of the readout. In qudits it is QND to the extent that off-diagonal contributions in Eq. (15) can be neglected. Yet, these terms slightly rotate the eigenstates of the isolated spin Hamiltonian with respect to those of the frequency shift term. If off-diagonal terms are included, the relevant commutator in Eq. (16) yields

$$\sum_{\beta_i=1}^{2S+1} E_{\beta} \Phi_{\beta} X^{\beta} = (X^{+,-} - X^{-,+}) \sum_{\alpha=\pm} \frac{(\lambda_x g_x)^2 E_{\alpha}}{E_{\alpha}^2 - \Omega^2}. \quad (20)$$

Note that the deviation from an ideal nondemolition measurement is, as we anticipated, a consequence of the magnetic anisotropy D . This can be seen if we take the limit $D \rightarrow 0$ in Eq. (20), which makes it vanish for $E_{\pm} = D \pm \xi_z$. Nevertheless, the correction to an ideal QND measurement is small, as it is proportional to λ_x^2 and to the average of the off-diagonal operators, $X^{\pm,\mp}$, which involve two spin-flip processes (also proportional to λ_x^2). Therefore, corrections become important only beyond the dispersive regime or for long timescales (i.e., when the spins have evolved in time, moving significantly away from the initial state ρ that is to be measured), and for all practical purposes, one can safely consider that the transmission readout is a QND measurement. Interestingly, it would also be possible to suppress this effect in some cases by aligning the external magnetic field along specific directions, in order to make Eq. (16) vanish. Concretely, in this case the working point $\xi_z = \sqrt{D^2 - \Omega^2}$ makes Eq. (20) go to zero.

We have presented a simple model where the fundamental features of magnetic circuit QED can be grasped in simple terms. However, models of artificial magnetic molecules can be more complex and contain a larger number of levels. For this reason, we now consider three cases of fundamentally different artificial magnetic molecules,

which are currently under study as interesting candidates for quantum technologies.

B. Single-ion magnet GdW₃₀

The inorganic molecular moiety GdW₃₀ encapsulates a single $S = 7/2$ Gd³⁺ ion with long spin coherence time. Gadolinium has some characteristic traits that make this system of particular interest: it has the largest spin of the periodic table and, because of its close to spherical 4*f* electronic shell, the zero-field splittings between spin levels are 1–2 orders of magnitude smaller than those found for other lanthanide or transition-metal ions. These properties combined provide a large set of levels with energies lying within the reach of microwave cavities. Besides, and due to its weak but yet nonzero magnetic anisotropy, different spin transitions also have different resonant frequencies and they can be independently addressed. Finally, any operation can be implemented by concatenation of the subset of transitions that can be induced by resonant microwave pulses. As a consequence, this molecule is equivalent to a universal three-qubit processor (since $2^3 = 2 \times 7/2 + 1$) [37]. Here we show that, in addition to all this, every state can be resolved by means of our dispersive readout proposal. The spin Hamiltonian of GdW₃₀ has longitudinal as well as in-plane magnetic anisotropy terms. It can be written as

$$\mathcal{H}_S = \frac{D}{3}O_2^0 + EO_2^2 - \mu_B g \vec{B} \cdot \vec{S} \quad (21)$$

with $O_2^0 = 3(S^z)^2 - S(S+1)$ and $O_2^2 = (S^x)^2 - (S^y)^2$. Experimental values are $D = 1.281$ GHz, $E = 0.294$ GHz, and $g = 2$. Typical spin decoherence times for this molecule are of the order of a few microseconds. This needs to be compared with the spin-photon coupling. The magnetic field produced by the vacuum fluctuations in a standard design of a superconducting resonator is around 0.1 nT. This gives an effective spin-photon coupling to each of the allowed spin transitions of the order of a few hertz, which is much smaller than the value required to discriminate resonances associated with different spin states in the dispersive regime. However, this problem can be mitigated by considering ensembles of molecules, which provide the scaling \sqrt{N} in the effective coupling [cf. Eq. (12)]. Considering a diluted single crystal containing only 1% of magnetic molecules dispersed in a diamagnetic host (for instance, the YW₃₀ derivative), the cavity would couple to approximately 1.6×10^{14} molecules, providing collective spin-photon couplings of the order of tens of megahertz.

Figure 4 (top) shows the energy levels as a function of magnetic field. In Fig. 4 (bottom) the transmission is plotted as a function of ω for a cavity with frequency $\Omega = 5$ GHz and a field configuration $\vec{B} = (1, 0.3, 0.3)b$ with $b = 0.1475$ T [vertical line in Fig. 4 (top)]. It shows

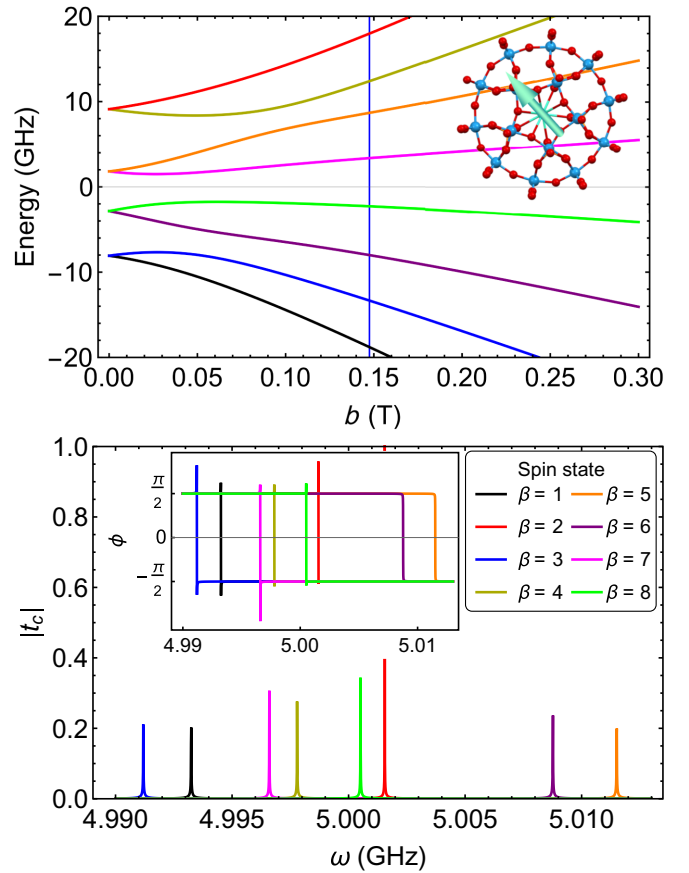


FIG. 4. Top: spin energy levels of GdW₃₀, shown in the inset, as a function of magnetic field b . The vertical blue line indicates the value chosen to calculate the transmission. Bottom: transmission versus ω for the different spin states of a crystal of $N = 1.6 \times 10^{14}$ GdW₃₀ molecules and a cavity frequency $\Omega = 5$ GHz. The inset shows the phase of the transmission for the same range of ω . The photon and spin decoherence rates take values $\gamma_i = 10^{-6}$ GHz and $\eta = 10^{-4}$ GHz.

that the transmission resonance is different for each state of the molecule and that the frequency shifts can be experimentally resolved, provided that the spin levels are predominantly homogeneously broadened. This is crucial for molecules with a large number of levels, where frequency crowding can hinder resolving between states and lead to similar transmission resonances. It is also very important to determine an adequate field configuration \vec{B} , where $d - 1$ frequency shifts are sufficiently large. Clearly, this highly depends on the magnetic anisotropy of the molecule and on the available frequencies of the resonator Ω . Nevertheless, if two or more levels cannot be resolved, repeating the process at different magnetic field values would allow us to completely determine the spin state. The inset in Fig. 4 shows again that the phase of the transmission can be used to perform the readout.

Unfortunately, in this particular molecular system the inhomogeneous broadening remains large (>100 MHz

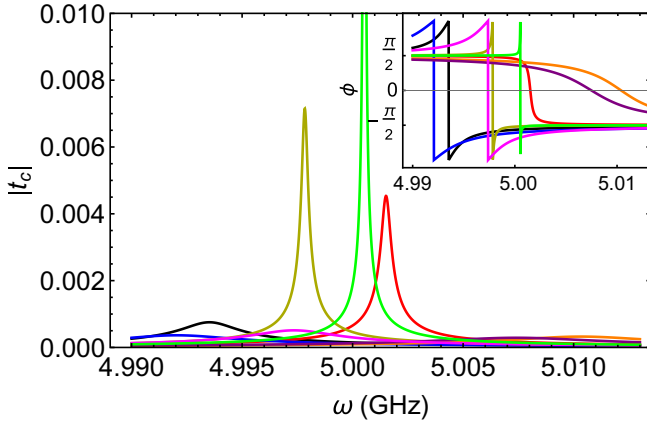


FIG. 5. Plot of $|t_c|$ versus ω for the same parameters as in Fig. 4, but with $\eta = 0.1$ GHz, which is the inhomogeneous broadening of the spin levels determined for diluted samples of GdW_{30} [37]. The transmission peaks are highly suppressed and they partially overlap. Still, information about the state can be extracted from the transmission phase (inset).

[37]) even for highly diluted crystals, probably as a result of strains in the magnetic anisotropy parameters associated with the presence of different metastable molecular conformations at low temperatures. As can be seen in Fig. 5 (cf. Fig. 4), the main consequences are the broadening and amplitude reduction of the peaks, as was previously seen in Fig. 3. This is due to the strengths of dissipative terms and the detuning of each transition from the resonator frequency. This limits, although it does not completely preclude, the ability to discriminate between different spin states.

Nevertheless, it is important that these results show what the dominant sources of error are to direct future research towards magnetic molecules with adequate properties for their manipulation in cavities.

C. Heterodimetallic [CeEr] lanthanide complex

The molecular dimer [CeEr] behaves, at sufficiently low T , as two weakly coupled anisotropic $S = 1/2$ spins, i.e., it deviates from the giant spin approximation. It provides a model situation to explore a system of two dissimilar, thus addressable, spin qubits. Their mutual coupling allows us to implement conditional two-qubit gates and ensures universal operations within the $d = 4$ Hilbert space [35]. This magnetic molecule can be described by the spin Hamiltonian [35]

$$\mathcal{H}_S = -\mu_B \sum_{i=1,2} \vec{B} \cdot \hat{g}_i \cdot \vec{S}_i - \frac{J_{12}}{g_{J1}g_{J2}} (\hat{g}_1 \cdot \vec{S}_1) \cdot (\hat{g}_2 \cdot \vec{S}_2), \quad (22)$$

where the effective gyromagnetic tensor of the i th spin ($i = 1, 2$ for Er and Ce, respectively) is given by

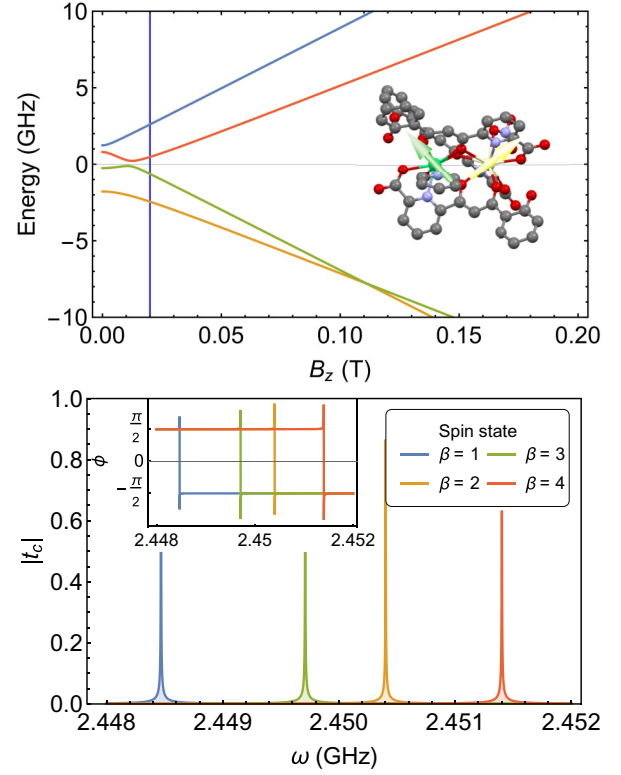


FIG. 6. Top: Spin energy levels of [CeEr], shown in the inset, as a function of magnetic field. Bottom: Transmission $|t_c|$ vs ω for a cavity frequency $\Omega = 2.45$ GHz and $B_z = 0.02$ T. The inset shows the phase of the transmission for the same frequency range. Parameters: $N = 2.7 \times 10^{14}$, $\gamma_i = 10^{-6}$ GHz and $\eta = 10^{-4}$ GHz.

$\hat{g}_1 = (1.8, 3.7, 10)$ and $\hat{g}_2 = (1, 1.75, 2.67)$, and the Landé factors are $g_{J1} = 6/5$ and $g_{J2} = 6/7$, respectively. For the spin-spin interaction, we have chosen a scalar form of the interaction tensor with $J_{12}/k_B = -0.015$ K, and for the field configuration, we choose \vec{B} to be aligned along the z axis of the Er spin. The anisotropy axis of the Ce spin then makes an angle of about $\theta = 70^\circ$ with respect to \vec{B} . For simplicity, we choose our frame of reference in such a way that the angle θ lies in the x - z plane. The dimer levels are plotted in Fig. 6 (top) as a function of the magnetic field.

When coupling to the cavity, the dimer molecule turns out to be slightly more complex than the previous discussed examples. This is due to the misalignment between the local anisotropies of both ions, which makes them couple differently with the cavity photons. The total Hamiltonian can be written as (see Appendix E for explicit expressions for each ion)

$$\mathcal{H} = \mathcal{H}_S + \mathcal{H}_c + (a^\dagger + a) \sum_{\vec{\alpha}} X^{\vec{\alpha}} \sum_i \vec{\epsilon} \cdot \hat{g}_i \cdot \langle \alpha_1 | \vec{S}_i | \alpha_2 \rangle, \quad (23)$$

where now \hat{g}_2 is a nondiagonal matrix and the $X^{\bar{\alpha}}$ are the exact eigenstates of the isolated dimer (i.e., they are many-body states of the two spins). Note that in this case the effective \hat{g} tensor measured in an experiment would be very different from that of the isolated ions and that it contains contributions from the interaction J_{12} . As in the previous case for the GdW₃₀ molecule, the coupling between a single molecule and the cavity is too small, and we must consider ensembles of molecules.

In Fig. 6 we show the transmission as a function of ω for a cavity of frequency $\Omega = 2.45$ GHz and longitudinal field $h_z = 0.02$ T. It shows that the frequency shift is large enough to be experimentally resolved. The inset shows that the phase ϕ , again, can be used for unequivocally determining the spin state of the molecule.

It is also important to discuss the role of the cavity Q factor in the readout. So far, we have assumed that spins decohere much faster than cavity photons, as is usually the case. This produces sharp peaks in the transmission at specific frequencies, which is one of the reasons why phase measurements are more robust to imperfections during the readout. This picture can change if the decoherence rate of the cavity, γ , is close to that of the spins, η . In this case, the transmission peaks associated with different spin states broaden and partially overlap (see the inset of Fig. 7). At any frequency close to one of these resonances, this gives rise to a continuous change in the transmission and produces the interesting behavior shown in Fig. 7, as a function of magnetic field. In this case, one can see that measuring the transmission at a single frequency $\omega = \Omega$ and for a single magnetic field value gives a different, nonzero outcome for each spin state. Eventually, this could allow performing a single-shot readout of the spin state

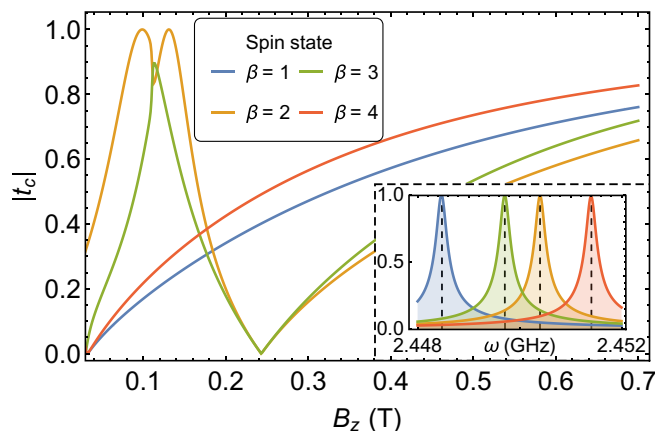


FIG. 7. Absolute value of the transmission for $\omega = \Omega$ as a function of the longitudinal field. We have considered a cavity with dissipative rates $\gamma_i = 10^{-4}$, which are of the order of T_2 for the molecule. The inset shows the broadening of the transmission peaks as a function of ω for $B_z = 0.02$ T.

provided that the transmission differences can be experimentally resolved. Obviously, a less coherent cavity also restricts the effective lifetime of the qudit state to which it is coupled. Yet, this coherence loss could be compensated by the reduction in the number of measurements required.

As we discussed in the case of GdW₃₀, all this applies to the case in which the spin line widths are dominated by the homogeneous broadening. Synthesizing single crystals hosting molecular dimers, such as CeEr, diluted in a diamagnetic host is still very challenging, whereas the use of frozen solutions leads to very broad resonances on account of the random distribution of anisotropy axes. This underlines the importance of using realistic calculations to guide the choice, and the design, of suitable candidates. A promising one is discussed in the next section.

D. ¹⁷³Yb-trensals: an electronuclear spin qudit

Experimentally, it has been shown that a single spin-photon interaction, of the order of kilohertz, can be achieved in constrained resonators [18], and that there are already molecular spins showing T_2 values in the vicinity of 1 ms [65]. However, as readout will likely be first performed in spin ensembles, the limiting factor will be the inhomogeneous broadening rather than T_2 , which will be difficult to reduce in the previous cases of GdW₃₀ and [CeEr]. For this reason, we now consider the case of ¹⁷³Yb-trensals, which combines a nuclear spin qudit ($I = 5/2$) coupled to an effective $S = 1/2$ electronic spin doublet.

In contrast with the previous examples, the photon coupling to the nuclear spin is much weaker than that to the electron spin, due to the small ratio between the nuclear and the electronic magneton, $\mu_N/\mu_B \ll 1$. However, the presence of a strong hyperfine interaction, characteristic of lanthanide ions, mediates the indirect coupling between the nuclear spin and the photons and, therefore, the manipulation of all the spin levels defining the qubit. This means that, in principle, it should be possible to perform the dispersive readout of all electronuclear spin states, including states differing only by their nuclear spin projection m_I . We now show that this is possible in practice. In addition, this molecular system has been considered as a good candidate for the implementation of quantum error correction codes [30,66], in which the nuclear spin helps to define the computational basis of the logical qubit and the electronic spin is exploited to detect errors. With this idea in mind, we now discuss how to readout the logical qubit states, and demonstrate that, due to the QND nature of the measurement, we could also detect errors to neighboring energy levels at any arbitrary time of the error correction protocol.

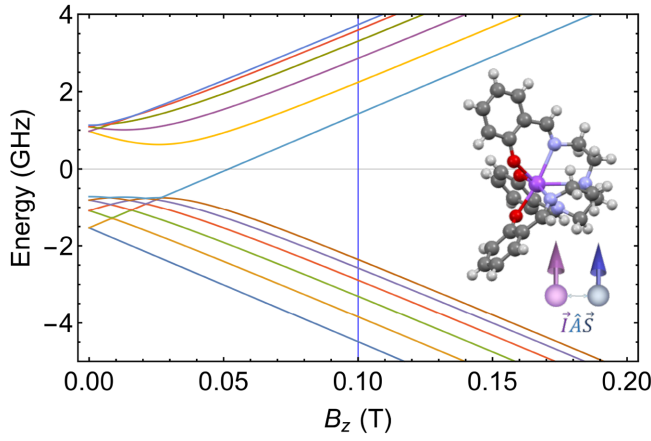


FIG. 8. Spectrum of the ^{173}Yb -trensral molecule as a function of B_z . The vertical (blue) line indicates the field chosen to perform the readout.

Let us first introduce the Hamiltonian for the ^{173}Yb -trensral molecule, which is given by

$$\mathcal{H}_S = \mu_B \vec{B} \cdot \hat{g} \cdot \vec{S} + \mu_N g_I \vec{B} \cdot \vec{I} + p I_z^2 + A_{\parallel} S_z I_z + A_{\perp} (S_x I_x + S_y I_y), \quad (24)$$

where the first line contains the coupling of the electronic and nuclear spin to the external magnetic field, where μ_N is the nuclear magneton, g_I is the nuclear g factor, and p describes the nuclear quadrupolar interaction, and the second line contains the anisotropic hyperfine interaction. From the experimental fitting of the parameters one finds that $\hat{g} = (g_{\perp}, g_{\perp}, g_{\parallel})$, $g_{\perp} = 2.935$, $g_{\parallel} = 4.225$, $g_I = -0.02592$, $A_{\parallel} = -0.897$ GHz, $A_{\perp} = -0.615$ GHz, and $p = -0.066$ GHz. In Fig. 8 we plot the spectrum of the ^{173}Yb -trensral molecule as a function of the longitudinal field. It shows how the magnetic field controls the hybridization of the electronic nuclear states.

Regarding the spin-photon coupling, the $\Lambda_{\vec{a}}$ tensor now takes a different form than in the previous cases, due to the presence of the nuclear spin. Concretely, the interaction Hamiltonian via the Zeeman term is given by

$$\mathcal{H}_I = (a^{\dagger} + a)(\vec{\lambda}_S \cdot \hat{g}_S \cdot \vec{S} + \vec{\lambda}_I \cdot \hat{g}_I \cdot \vec{I}). \quad (25)$$

Although we consider all terms in Eq. (25), it is also a good approximation to neglect the contribution proportional to the nuclear magneton $\vec{\lambda}_I$.

For isotopically pure crystals of ^{173}Yb -trensral with a 1% concentration, it is possible to estimate, from experimental measurements [67], a collective spin-photon coupling of the order of $\lambda_S^x = 20$ MHz, which is enough to achieve coherent coupling. Simultaneously, the inhomogeneous broadening is of the order of $\eta = 12$ MHz for this concentration.

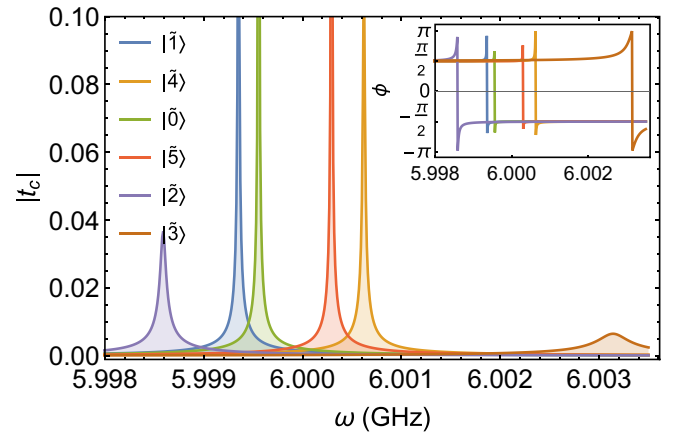


FIG. 9. Resonator transmission for the ground-state multiplet at $B_z = 0.1$ T and $\Omega = 6$ GHz. The states $|\tilde{1}\rangle$ and $|\tilde{4}\rangle$ encode the logical qubits with quantum error correction, but the other states can also be detected. The inset shows the phase measurement, which is more robust for the case of damped transmission peaks, as one can see for state $|\tilde{3}\rangle$. Parameters are $\gamma = 10^{-3}$ MHz, $\eta = 12$ MHz, and collective spin-photon coupling $\lambda_S^x = 20$ MHz.

The use of ^{173}Yb -trensral as a qubit with embedded error correction exploits the six levels multiplet associated with the electronic spin projection $m_S = -1/2$, which allows us to implement a minimal code for protection against single-amplitude or phase errors [29]. For this, one defines the logical qubit in terms of the states $|\tilde{1}\rangle = |-\frac{1}{2}, -\frac{3}{2}\rangle$ and $|\tilde{4}\rangle = |-\frac{1}{2}, \frac{3}{2}\rangle$, while all the other states in the multiplet are auxiliary to implement the code. Therefore, we are primarily interested in reading out states $|\tilde{1}\rangle$ and $|\tilde{4}\rangle$, to know the state of the logical qubit. Nevertheless, our readout protocol should also allow us to detect the other states in the multiplet, in case we want to study the inner workings of the error correction code or the influence of more complex errors produced, e.g., by correlated errors with other spins [68,69]. We show in Fig. 9 the transmission calculated for the different qudit states and the experimental parameters. Importantly, the logical qubit peaks are well separated, indicating that the qubit can be measured using the dispersive readout. This also implies that, although the level broadening is of the order of 12 MHz, a high resonator Q factor is more important. Actually, the dominant effect of the spectral broadening is to reduce the height of the peaks, which can be mitigated by performing phase measurements. Furthermore, the other states in the multiplet can also be measured, allowing us to detect and correct errors.

IV. CONCLUSIONS

We have presented a general framework to study the transmission of a superconducting cavity coupled to magnetic molecules of arbitrary spin in the dispersive regime.

Our framework incorporates their multilevel structure and the influence of the magnetic anisotropy, which is ubiquitous in these molecules. It is valid in both the strong- and weak-coupling regimes of spin-photon interaction. Besides, it can be adapted to more complex situations involving several coupled spins within each molecule. We have shown that the transmission depends on the spin state in a way that allows a univocal determination of this state. Our results provide a generalization of the well-known dispersive readout of qubits, which is broadly used in different quantum computing schemes. Therefore, molecular spin qudits can not only be coherently controlled to implement different quantum gates or protocols, but the results can also be readout with technologically available methods.

The multilevel structure of the qudit however introduces some changes to the readout protocol: $d - 1$ measurement pulses with judiciously chosen frequencies, instead of just one as in the case of qubits, are required to determine the spin state. Besides this method, we have shown that a single-shot readout protocol is also feasible, provided that the bare resonator linewidth be comparable to the decoherence rate of the spin qudit.

In addition, there are qualitatively additional features. In general, the magnetic anisotropy, which leads to the nonlinear arrangement of the spin qudit levels, affects the nondemolition nature of the dispersive readout. This property can, however, be restored by an appropriate control of the magnetic fields coupled to the molecule. We have also developed an effective Hamiltonian to describe the coupled qudit-cavity system that generalizes the well-known effective spin-photon interaction Hamiltonian for $S = 1/2$ to arbitrary spin with nonlinear magnetic anisotropy terms. This formalism can also be helpful to study the state dynamics, for the implementation of quantum gates and protocols [70]. It also provides a theoretical framework to analyze other applications of the cavity-spin coupling in the dispersive regime, e.g., to perform magnetic spectroscopy measurements [71].

As an application and illustration of our method, we have considered three relevant examples of molecular spin qudits currently under study. The first is a Gd-based single-ion magnet with $S = 7/2$ that encodes three qubits and that was used to implement a Toffoli gate. The second is a molecular dimer [CeEr] in which it is possible to define a fully addressable two-qubit system and where a controlled-NOT gate has been implemented. The third corresponds to the molecule of ^{173}Yb -trensal with $d = 12$ electronuclear spin states, where error correction can be implemented. We have shown that the cavity transmission can be used to readout the spin qudit states, although the inhomogeneous broadening might limit the application of this method in the first two systems. For Yb-trensal, we have shown that coupling of cavity photons to electronic spin transitions, in the range of a few gigahertz, allows reading out the nuclear spin states. This effect results from the strong hyperfine

interaction that characterizes lanthanide spin qubits, and might considerably simplify the implementation of proof-of-concept experiments in this and related systems. The theory will likely provide a useful guide for the design of suitable molecular spin qudits, which should combine a proper level anharmonicity, a not too large distribution of resonant frequencies to make frequency shifts associated with all states observable, and good material properties (e.g., a sufficiently low inhomogeneous broadening).

ACKNOWLEDGMENTS

We acknowledge funding from Spanish MCIN/AEI/10.13039/501100011033/ Grants No. PGC2018-094792-B-I00, No. RTI2018-096075-B-C21, and No. PCI2018-093116 (MCIU/AEI/FEDER, UE), the European Union's Horizon 2020 research and innovation programme (QUANTERA project SUMO and FET-OPEN project FATMOLS, Grant No. 862893), the Gobierno de Aragón Grant No. E09-17R-Q-MAD, and the CSIC Quantum Technology Platform PT-001.

APPENDIX A: CAVITY TRANSMISSION FOR AN ENSEMBLE OF MAGNETIC MOLECULES

Here we derive the cavity transmission for the case of an ensemble of molecules, using the equation of motion technique. We start from the full Hamiltonian

$$\mathcal{H} = \mathcal{H}_B + \mathcal{H}_c + \mathcal{H}_S + \mathcal{H}_I, \quad (\text{A1})$$

where $\mathcal{H}_S = \sum_{i=1}^N \sum_{\alpha=1}^{2S+1} E_{\alpha} X_i^{\alpha,\alpha}$, $\mathcal{H}_I = (a^{\dagger} + a) \sum_{i=1}^N \sum_{\alpha=1}^{2S+1} \Lambda_i^{\alpha} X_i^{\alpha}$, $\mathcal{H}_c = \Omega a^{\dagger} a$, and \mathcal{H}_B is the Hamiltonian for the modes in the transmission line, which can be written as

$$\begin{aligned} \mathcal{H}_B = & \sum_l \int_{-\infty}^{\infty} \omega b_{\omega,l}^{\dagger} b_{\omega,l} d\omega \\ & + i \sum_l \int_{-\infty}^{\infty} d\omega [\kappa_l(\omega) b_{\omega,l}^{\dagger} a - \kappa_l^*(\omega) a^{\dagger} b_{\omega,l}] \end{aligned} \quad (\text{A2})$$

with $b_{\omega,l}$ the photon operator at energy ω and port l , and $\kappa_l(\omega) = \sqrt{\gamma_l/2\pi}$ under the first Markov approximation. To integrate out the transmission line modes, we calculate of the Heisenberg equation of motion for the transmission line, i.e.,

$$\partial_t b_{\omega,l}(t) = -i\omega b_{\omega,l}(t) + \sqrt{\frac{\gamma_l}{2\pi}} a(t), \quad (\text{A3})$$

which can be directly integrated to give

$$b_{\omega,l}(t) = b_{\omega,l}(t_0) e^{-i\omega(t-t_0)} + \sqrt{\frac{\gamma_l}{2\pi}} \int_{t_0}^t e^{-i\omega(t-\tau)} a(\tau) d\tau \quad (\text{A4})$$

and leads to the standard Langevin equation for the cavity modes (we define the total dissipation rate $\gamma = \sum_l \gamma_l$):

$$\begin{aligned} \partial_t a(t) = & -i\left(\Omega - i\frac{\gamma}{2}\right)a(t) - i\sum_{i=1}^N \sum_{\bar{\alpha}=1}^{2S+1} \Lambda_i^{\bar{\alpha}} X_i^{\bar{\alpha}}(t) \\ & - \sum_l \sqrt{\gamma_l} b_{\text{in},l}(t) \end{aligned} \quad (\text{A5})$$

with the standard definition for the input modes given by

$$b_{\text{in},l}(t) = \frac{1}{\sqrt{2\pi}} \int_{-\infty}^{\infty} d\omega e^{-i\omega(t-t_0)} b_{\omega,l}(t_0). \quad (\text{A6})$$

To close the system of equations, we calculate the Heisenberg equation of motion for an arbitrary Hubbard operator:

$$\begin{aligned} \partial_t X_i^{\bar{\alpha}}(t) = & iE_{\bar{\alpha}} X_i^{\bar{\alpha}}(t) + i(a(t) + a^\dagger(t)) \sum_{\mu} (\Lambda_i^{\mu,\alpha_1} X_i^{\mu,\alpha_2}(t) \\ & - \Lambda_i^{\alpha_2,\mu} X_i^{\alpha_1,\mu}(t)). \end{aligned} \quad (\text{A7})$$

This requires a truncation scheme to close the system of equations (because it couples to additional many-body operators such as $aX^{\alpha_1,\mu}$). In addition, note that we have assumed that the energies of the spins are all equal, because their chemical synthesis produces identical molecules and the external magnetic field is homogeneous. However, this could not be the case due to local substrate effects or if the system under consideration is not made of identical qudits. In that case the calculation just requires also defining a continuous spectral density to solve the coupled equations of motion.

As experiments typically display weak coupling between individual spins and the cavity, one can write the

following decomposition to separate the photonic and the spin part of the many-body operators:

$$\begin{aligned} aX^{\mu,\nu} = & a\langle X^{\mu,\nu} \rangle + \langle a \rangle X^{\mu,\nu} + \delta a \delta X^{\mu,\nu} \\ \simeq & a\langle X^{\mu,\nu} \rangle \delta_{\mu,\nu}. \end{aligned} \quad (\text{A8})$$

This approximation is only valid for weak interactions, but its valid to describe the weak- and strong-coupling regimes [58]. The reasons are that, in this limit, fluctuations $\delta a \delta X^{\mu,\nu}$ are very small (this can be argued in terms of a mean field description), and that off-diagonal averages are also small compared with diagonal ones (note that the Hamiltonian is completely diagonal in the absence of coupling). This allows us to neglect the averages $\langle a \rangle$, $\langle a^\dagger \rangle$, and $\langle X^{\mu,\nu} \rangle$ for $\mu \neq \nu$. In addition, we neglect the term proportional to $a^\dagger \langle X^{\mu,\nu} \rangle$, because its correction is of higher order. This is not strictly necessary to close the set of equations, but allows us to obtain more compact expressions. In summary, after a Fourier transform, the solution for the equation of motion of an arbitrary Hubbard operator takes the form

$$X_i^{\bar{\alpha}}(\omega) \simeq -a \frac{\Lambda_i^{\alpha_2,\alpha_1}}{\omega + E_{\bar{\alpha}}} (\langle X_i^{\alpha_2,\alpha_2} \rangle - \langle X_i^{\alpha_1,\alpha_1} \rangle). \quad (\text{A9})$$

Finally, as a last assumption to obtain a compact expression for the transmission, we consider the system in a diagonal density matrix in the basis of Hubbard operators $\rho = \sum_{\alpha=1}^{2S+1} p_\alpha X^{\alpha,\alpha}$ for all the different molecules in the ensemble. This is adequate due to the state preparation carried out in the experimental setups. All these assumptions result in the final expression for the cavity mode:

$$a(\omega) = \frac{i \sum_l \sqrt{\gamma_l} b_{\text{in},l}(\omega)}{\Omega - \omega - i\gamma/2 + \sum_{i=1}^N \sum_{\bar{\alpha}=1}^{2S+1} p_{\bar{\alpha}} |\Lambda_i^{\bar{\alpha}}|^2 / (\omega + E_{\bar{\alpha}} + i\eta)}. \quad (\text{A10})$$

Here $|\Lambda_i^{\bar{\alpha}}|^2 = \Lambda_i^{\alpha_1,\alpha_2} \Lambda_i^{\alpha_2,\alpha_1}$, $E_{\bar{\alpha}} = E_{\alpha_1} - E_{\alpha_2}$, $p_{\bar{\alpha}} = p_{\alpha_1} - p_{\alpha_2}$, and η is the phenomenological spectral broadening of the spin energy levels. To obtain the cavity transmission, one just needs to make use of the standard input-output relation in $t_c = \langle b_{\text{out},2} \rangle / \langle b_{\text{in},1} \rangle$. This result demonstrates that the frequency shift produced by the interaction between the cavity mode and the ensemble of molecules is enhanced by a factor N with respect to the case of a single molecule. Moreover, although the derivation requires making an assumptions about the coupling strength between a single spin and the cavity photons in the dispersive regime

(i.e., for an off-resonant condition between spin transitions and the cavity), it does not require a condition with respect to γ or η , which allows us to explore both the weak- and strong-coupling regimes. In addition, if one is interested in going beyond the strong-coupling regime, the formula remains valid by just considering a mean field basis [59].

To explicitly see the enhancement in the cavity frequency shift, assume that all the molecules are prepared in state β (i.e., $p_\alpha = 1$ for $\alpha = \beta$; otherwise, $p_\alpha = 0$). Then, the sum in the denominator of the transmission contains only two terms:

$$t_c(\omega) = \frac{i\sqrt{\gamma_1\gamma_2}}{\Omega - \omega - i\gamma/2 + \sum_{i=1}^N \sum_{\alpha=1}^{2S+1} [\Lambda_i^{\beta,\alpha} \Lambda_i^{\alpha,\beta} / (\omega + E_\beta - E_\alpha + i\eta) - \Lambda_i^{\alpha,\beta} \Lambda_i^{\beta,\alpha} / (\omega + E_\alpha - E_\beta + i\eta)]}. \quad (\text{A11})$$

Reorganizing the denominator we can write

$$t_c(\omega) = \frac{i\sqrt{\gamma_1\gamma_2}}{\Omega - \omega - i\gamma/2 + \sum_{i=1}^N \sum_{\alpha=1}^{2S+1} 2|\Lambda_i^{\alpha,\beta}|^2(E_\alpha - E_\beta) / [(\omega + i\eta)^2 - (E_\alpha - E_\beta)^2]}, \quad (\text{A12})$$

where it is clear that the shift in the frequency photon measured at ω is

$$\delta\tilde{\Omega}_\beta(\omega) = \sum_{i=1}^N \sum_{\alpha=1}^{2S+1} \frac{2|\Lambda_i^{\alpha,\beta}|^2 E_{\alpha,\beta}}{(\omega + i\eta)^2 - E_{\alpha,\beta}^2}. \quad (\text{A13})$$

APPENDIX B: DERIVATION OF THE EFFECTIVE HAMILTONIAN AND CHECK FOR THE QUBIT CASE

The calculation of the Schrieffer-Wolff transformation requires first finding the ansatz for the transformation \mathcal{S} . For this, it is common to find an operator form from the commutator $[\mathcal{H}_0, \mathcal{H}_I]$. This results in the following expression for the transformation:

$$\mathcal{S} = \sum_{\vec{\beta}=1}^{2S+1} (\Gamma_{+}^{\vec{\beta}} a^\dagger + \Gamma_{-}^{\vec{\beta}} a) X^{\vec{\beta}} \quad (\text{B1})$$

with $\Gamma_{\pm}^{\vec{\beta}} = \Lambda_{\vec{\beta}}/E_{\vec{\beta}} \pm \Omega$. The calculation of the effective Hamiltonian to second order in $\Lambda_{\vec{\alpha}}$, $\tilde{\mathcal{H}} \simeq \mathcal{H}_0 + \frac{1}{2}[\mathcal{S}, \mathcal{H}_I]$, is obtained from the calculation of the commutator $[\mathcal{S}, \mathcal{H}_I]$, which yields

$$\begin{aligned} [\mathcal{S}, \mathcal{H}_I] &= 2a^\dagger a \sum_{\beta_i, \alpha=1}^{2S+1} \Lambda_{\beta_1, \alpha} \Lambda_{\alpha, \beta_2} \left(\frac{E_{\beta_1, \alpha}}{E_{\beta_1, \alpha}^2 - \Omega^2} - \frac{E_{\alpha, \beta_2}}{E_{\alpha, \beta_2}^2 - \Omega^2} \right) X^{\vec{\beta}} \\ &+ \sum_{\beta_i, \alpha=1}^{2S+1} \Lambda_{\beta_1, \alpha} \Lambda_{\alpha, \beta_2} \left(\frac{1}{E_{\beta_1, \alpha} - \Omega} - \frac{1}{E_{\alpha, \beta_2} + \Omega} \right) X^{\vec{\beta}} \\ &+ (a^\dagger)^2 \sum_{\beta_i, \alpha=1}^{2S+1} \Lambda_{\beta_1, \alpha} \Lambda_{\alpha, \beta_2} \left(\frac{1}{E_{\beta_1, \alpha} + \Omega} - \frac{1}{E_{\alpha, \beta_2} + \Omega} \right) X^{\vec{\beta}} \\ &+ a^2 \sum_{\beta_i, \alpha=1}^{2S+1} \Lambda_{\beta_1, \alpha} \Lambda_{\alpha, \beta_2} \left(\frac{1}{E_{\beta_1, \alpha} - \Omega} - \frac{1}{E_{\alpha, \beta_2} - \Omega} \right) X^{\vec{\beta}}. \end{aligned} \quad (\text{B2})$$

The final form of the effective Hamiltonian is obtained by adding the unperturbed terms, resulting in the expression

$$\begin{aligned} \tilde{\mathcal{H}} &\simeq \sum_{\alpha} E_{\alpha} X^{\alpha, \alpha} + \frac{1}{2} \sum_{\beta_i, \alpha=1}^{2S+1} \Lambda_{\beta_1, \alpha} \Lambda_{\alpha, \beta_2} \left(\frac{1}{E_{\beta_1, \alpha} - \Omega} + \frac{1}{E_{\beta_2, \alpha} - \Omega} \right) X^{\vec{\beta}} \\ &+ \Omega a^\dagger a + a^\dagger a \sum_{\beta_i, \alpha=1}^{2S+1} \Lambda_{\beta_1, \alpha} \Lambda_{\alpha, \beta_2} \left(\frac{E_{\beta_1, \alpha}}{E_{\beta_1, \alpha}^2 - \Omega^2} + \frac{E_{\beta_2, \alpha}}{E_{\beta_2, \alpha}^2 - \Omega^2} \right) X^{\vec{\beta}} \\ &+ \frac{1}{2} (a^\dagger)^2 \sum_{\beta_i, \alpha=1}^{2S+1} \Lambda_{\beta_1, \alpha} \Lambda_{\alpha, \beta_2} \left(\frac{1}{E_{\beta_1, \alpha} + \Omega} + \frac{1}{E_{\beta_2, \alpha} - \Omega} \right) X^{\vec{\beta}} \\ &+ \frac{1}{2} a^2 \sum_{\beta_i, \alpha=1}^{2S+1} \Lambda_{\beta_1, \alpha} \Lambda_{\alpha, \beta_2} \left(\frac{1}{E_{\beta_1, \alpha} - \Omega} + \frac{1}{E_{\beta_2, \alpha} + \Omega} \right) X^{\vec{\beta}}. \end{aligned} \quad (\text{B3})$$

This Hamiltonian is valid up to second order in $\Lambda_{\bar{\alpha}}$ and has a large number of contributions, including second-order photon processes. Nevertheless, a simpler form can be obtained if we consider that diagonal averages $\langle X^{\alpha,\alpha} \rangle$ and $\langle a^\dagger a \rangle$ dominate over off-diagonal ones. This is a good approximation if the artificial molecule is weakly perturbed by the interaction with the cavity (however, if one is interested in the time evolution of the system, it might be important to include the off-diagonal terms to capture the long-time behavior). Therefore, we can write the final form of the Hamiltonian used in the main text as

$$\begin{aligned} \tilde{\mathcal{H}} \simeq & \sum_{\alpha} E_{\alpha} X^{\alpha,\alpha} + \sum_{\alpha,\beta=1}^{2S+1} \frac{|\Lambda_{\alpha,\beta}|^2}{E_{\alpha,\beta} - \Omega} X^{\alpha,\alpha} \\ & + a^\dagger a \left(\Omega + 2 \sum_{\alpha,\beta=1}^{2S+1} \frac{E_{\alpha,\beta} |\Lambda_{\alpha,\beta}|^2}{E_{\alpha,\beta}^2 - \Omega^2} X^{\alpha,\alpha} \right), \end{aligned} \quad (\text{B4})$$

where we have defined $|\Lambda_{\alpha,\beta}|^2 = \Lambda_{\alpha,\beta} \Lambda_{\beta,\alpha}$.

As a check, we can reproduce the case of several qubits interacting with a single photonic mode in a cavity:

$$\begin{aligned} H &= \sum_i \frac{\Delta_i}{2} \sigma_i^z + \Omega a^\dagger a + (a^\dagger + a) \sum_i g_i \sigma_i^x \\ &= \sum_i \frac{\Delta_i}{2} (X_i^{+,+} - X_i^{-,-}) + \Omega a^\dagger a \\ &+ (a^\dagger + a) \sum_i g_i (X_i^{+,-} + X_i^{-,+}). \end{aligned} \quad (\text{B5})$$

Inserting these couplings into the expression for the effective Hamiltonian we find that the Schrieffer-Wolff transformation is given by

$$\mathcal{S} = \sum_j g_j \left(\frac{a^\dagger X_j^{+,-} - a X_j^{-,+}}{\Delta_j + \Omega} + \frac{a X_j^{+,-} - a^\dagger X_j^{-,+}}{\Delta_j - \Omega} \right) \quad (\text{B6})$$

and the effective Hamiltonian by

$$\begin{aligned} \tilde{\mathcal{H}} &= \sum_i \frac{\Delta_i}{2} (X_i^{+,+} - X_i^{-,-}) \\ &+ \sum_i g_i^2 \left(\frac{X_i^{+,+}}{\Delta_i - \Omega} - \frac{X_i^{-,-}}{\Delta_i + \Omega} \right) \end{aligned}$$

$$\begin{aligned} &+ a^\dagger a \left[\Omega + \sum_i \frac{2\Delta_i g_i^2}{\Delta_i^2 - \Omega^2} (X_i^{+,+} - X_i^{-,-}) \right] \\ &+ (a^\dagger a^\dagger + aa) \sum_i \frac{\Delta_i g_i^2}{\Delta_i^2 - \Omega^2} (X_i^{+,+} - X_i^{-,-}) \\ &+ \sum_{ij \neq i} \frac{\Omega g_i g_j}{\Delta_j^2 - \Omega^2} (X_i^{+,-} + X_i^{-,+}) (X_j^{+,-} + X_j^{-,+}). \end{aligned} \quad (\text{B7})$$

Importantly, note how by neglecting off-diagonal contributions, we eliminate the quadratic photon terms a^2 and $(a^\dagger)^2$, but also the effective qubit-qubit interaction commonly used for quantum gates engineering. This is unimportant for the current case of quantum spectroscopy, where we are interested in the readout of the qubits state. The main reason is that readout is a fast process and the qubits do not have enough time to entangle via the effective interaction, which takes a time of the order of $\tau \sim g_i^{-2}$. However, if one is interested in effective interactions or these timescales, it will be important to keep off-diagonal terms as well [69,70].

APPENDIX C: NONDEMOLITION MEASUREMENT

The calculation of the commutator between the unperturbed spin Hamiltonian and the photon frequency shift term results in

$$[\mathcal{H}_S, \tilde{\mathcal{V}}] = \sum_{\beta=1}^{2S+1} E_{\bar{\beta}} \Phi_{\bar{\beta}} X^{\bar{\beta}}, \quad (\text{C1})$$

where

$$\tilde{\mathcal{V}} = \sum_{\beta,\alpha=1}^{2S+1} \Lambda_{\beta_1,\alpha} \Lambda_{\alpha,\beta_2} \left(\frac{E_{\beta_1,\alpha}}{E_{\beta_1,\alpha}^2 - \Omega^2} + \frac{E_{\beta_2,\alpha}}{E_{\beta_2,\alpha}^2 - \Omega^2} \right) X^{\bar{\beta}} \quad (\text{C2})$$

is the effective spin-photon interaction in Eq. (B3) and

$$\Phi_{\bar{\beta}} = \sum_{\alpha=1}^{2S+1} \Lambda_{\beta_1,\alpha} \Lambda_{\alpha,\beta_2} \left(\frac{E_{\beta_1,\alpha}}{E_{\beta_1,\alpha}^2 - \Omega^2} + \frac{E_{\beta_2,\alpha}}{E_{\beta_2,\alpha}^2 - \Omega^2} \right). \quad (\text{C3})$$

This expression is valid up to second order in $\Lambda_{\bar{\beta}}$ and indicates that in general the readout will not be a non-demolition measurement. To analyze this result in detail, we

can consider the qubit case

$$\sum_{\beta_i=1}^{2S+1} E_{\bar{\beta}} \Phi_{\bar{\beta}} X^{\bar{\beta}} = E_{+,-}^2 \frac{\Lambda_{-,-} - \Lambda_{+,+}}{E_{+,-}^2 - \Omega^2} \times (\Lambda_{+,-} X^{+,-} - \Lambda_{-,+} X^{-,+}), \quad (\text{C4})$$

which indicates that only if the spin-photon interaction is purely transversal (i.e., if $\Lambda_{\alpha,\alpha} = 0$) is the readout a non-demolition measurement. Crucially, these extra terms can be compensated by just rotating the unperturbed part of the Hamiltonian in such a way that the interaction term becomes purely transverse to the qubit quantization axis.

APPENDIX D: MOLECULE WITH SPIN $S = 1$

We consider an $S = 1$ molecule with uniaxial anisotropy and Hamiltonian

$$\mathcal{H} = D(S^z)^2 + \xi_z S^z + \Omega a^\dagger a + \lambda_x g_x (a^\dagger + a) S^x. \quad (\text{D1})$$

From the Hamiltonian, we can obtain the relevant unperturbed energies $E_{\pm} = D \pm \xi_z$ and $E_0 = 0$, and the elements of the interaction tensor

$$\Lambda_{\bar{\alpha}} = \frac{\lambda_x g_x}{2} \sqrt{2 - \alpha_1 \alpha_2} (\delta_{\alpha_1, \alpha_2 + 1} + \delta_{\alpha_2, \alpha_1 + 1}). \quad (\text{D2})$$

Then, inserting this values into Eq. (15), we can calculate the full effective Hamiltonian

$$\begin{aligned} \tilde{\mathcal{H}} \simeq & \Omega a^\dagger a - 4 \left(\frac{\lambda_x g_x}{2} \right)^2 \left[\frac{D + \Omega}{(D + \Omega)^2 - \xi_z^2} + a^\dagger a \left(\frac{D - \xi_z}{(D - \xi_z)^2 - \Omega^2} + \frac{D + \xi_z}{(D + \xi_z)^2 - \Omega^2} \right) \right] X^{0,0} \\ & + \left[D + \xi_z + \left(\frac{\lambda_x g_x}{2} \right)^2 \left(\frac{2}{D + \xi_z - \Omega} + a^\dagger a \frac{4(D + \xi_z)}{(D + \xi_z)^2 - \Omega^2} \right) \right] X^{+,+} \\ & + \left[D - \xi_z + \left(\frac{\lambda_x g_x}{2} \right)^2 \left(\frac{2}{D - \xi_z - \Omega} + a^\dagger a \frac{4(D - \xi_z)}{(D - \xi_z)^2 - \Omega^2} \right) \right] X^{-,-} \\ & + 2 \left(\frac{\lambda_x g_x}{2} \right)^2 \left[\frac{D - \Omega}{(D - \Omega)^2 - \xi_z^2} + a^\dagger a \left(\frac{D - \xi_z}{(D - \xi_z)^2 - \Omega^2} + \frac{D + \xi_z}{(D + \xi_z)^2 - \Omega^2} \right) \right] (X^{-,+} + X^{+,-}), \end{aligned} \quad (\text{D3})$$

where, as described in the main text, we have neglected second-order photon terms, but we have now kept the second-order transition operators $X^{\pm,\mp}$ to check the deviation from a QND measurement. Importantly, one can see how each spin subspace is affected differently by the coupling with the cavity, due to the influence of the nonlinear

anisotropy D . From this expression, it is easy to extract the frequency shifts described in the main text.

Finally, we can calculate the deviation from a perfect QND measurement by calculating the commutation between the unperturbed spin Hamiltonian and the frequency shift term. This yields

$$\begin{aligned} \sum_{\beta_i=1}^{2S+1} E_{\bar{\beta}} \Phi_{\bar{\beta}} X^{\bar{\beta}} &= 2 \left(\frac{\lambda_x g_x}{2} \right)^2 \left(\frac{E_+}{E_+^2 - \Omega^2} + \frac{E_-}{E_-^2 - \Omega^2} \right) (E_{+,-} X^{+,-} + E_{-,+} X^{-,+}) \\ &= 4 \xi_z \left(\frac{\lambda_x g_x}{2} \right)^2 \left(\frac{D + \xi_z}{(D + \xi_z)^2 - \Omega^2} + \frac{D - \xi_z}{(D - \xi_z)^2 - \Omega^2} \right) (X^{+,-} - X^{-,+}), \end{aligned} \quad (\text{D4})$$

where we have used

$$\Phi_{\bar{\beta}} = \sum_{\alpha=1}^{2S+1} \Lambda_{\beta_1, \alpha} \Lambda_{\alpha, \beta_2} \left(\frac{E_{\beta_1, \alpha}}{E_{\beta_1, \alpha}^2 - \Omega^2} + \frac{E_{\beta_2, \alpha}}{E_{\beta_2, \alpha}^2 - \Omega^2} \right). \quad (\text{D5})$$

Note that if $D \rightarrow 0$ then the commutator vanishes, indicating that the measurement is QND, to second order in $\Lambda_{\bar{\alpha}}$. Therefore, we can conclude that even for this case with purely longitudinal anisotropy and fully transverse interaction, the measurement is not QND due to the

presence of the nonlinear term $(S^z)^2$. Nevertheless, the noncommutativity is proportional to $(\lambda_x g_x)^2$, which is small, times the second-order transition operators $X^{\pm, \mp}$, whose expectation value is also small in the weak-coupling regime. Hence, for all practical purposes, it might be possible to neglect this effect during the readout, but nevertheless it should be estimated.

APPENDIX E: HETERODIMETALLIC [CeEr] LANTHANIDE COMPLEX

This molecule has the special feature of being an ionic dimer. From the experiment, it is possible to find the parameters for the diagonal form of the $\hat{g}_{1,2}$ tensor in each ion independently by fitting. However, the molecule accommodates the two ions with a relative orientation that has been estimated to be of the order of $\theta = 70^\circ$. This implies that the calculation of the eigenstates of the isolated molecule requires rotating \hat{g}_2 for the Ce ion. We consider a rotation in the x - z plane implemented by the matrix

$$\hat{R} = \begin{pmatrix} \cos \theta & 0 & \sin \theta \\ 0 & 1 & 0 \\ -\sin \theta & 0 & \cos \theta \end{pmatrix}, \quad (\text{E1})$$

which transforms \hat{g}_2 into the form

$$\hat{g}_2 = \begin{pmatrix} g_2^x \cos^2 \theta + g_2^z \sin^2 \theta & 0 & (g_2^z - g_2^x) \cos \theta \sin \theta \\ 0 & g_2^y & 0 \\ (g_2^z - g_2^x) \cos \theta \sin \theta & 0 & g_2^z \cos^2 \theta + g_2^x \sin^2 \theta \end{pmatrix}. \quad (\text{E2})$$

This allows us to write the Zeeman term as

$$H_Z = -\mu_B B_z [g_1^z S_1^z + (g_2^z \cos^2 \theta + g_2^x \sin^2 \theta) S_2^z] - \mu_B B_z (g_2^z - g_2^x) \cos \theta \sin \theta S_2^x. \quad (\text{E3})$$

In addition, we assume that the interaction tensor is scalar (lowest-order approximation, where each spin reacts to the effective magnetic field produced by the other), which means that the interaction Hamiltonian can be written as

$$V = -\frac{J_{12}}{g_{J1} g_{J2}} g_1^x (g_2^x \cos^2 \theta + g_2^z \sin^2 \theta) S_1^x S_2^x - \frac{J_{12}}{g_{J1} g_{J2}} g_1^y g_2^y S_1^y S_2^y - \frac{J_{12}}{g_{J1} g_{J2}} g_1^z (g_2^z \cos^2 \theta + g_2^x \sin^2 \theta) S_1^z S_2^z - \frac{J_{12}}{g_{J1} g_{J2}} \cos \theta \sin \theta (g_2^z - g_2^x) (g_1^x S_1^x S_2^z + g_1^z S_1^z S_2^x). \quad (\text{E4})$$

Finally, the coupling with the cavity photons must include the relative angle between the two ions, resulting in the

form

$$\sum_i \vec{\epsilon} \cdot \hat{g}_i \cdot \vec{S}_i = \epsilon_x g_1^x S_1^x + \epsilon_y (g_1^y S_1^y + g_2^y S_2^y) + \epsilon_z g_1^z S_1^z + (g_2^x \cos^2 \theta + g_2^z \sin^2 \theta) \epsilon_x S_2^x + (g_2^z \cos^2 \theta + g_2^x \sin^2 \theta) \epsilon_z S_2^z + (g_2^z - g_2^x) \cos \theta \sin \theta (\epsilon_z S_2^x + \epsilon_x S_2^z). \quad (\text{E5})$$

These are the main manipulations used to obtain the effective Hamiltonian for the dimer coupled to the cavity photons.

-
- [1] A. Wallraff, D. I. Schuster, A. Blais, L. Frunzio, R.-S. Huang, J. Majer, S. Kumar, S. M. Girvin, and R. J. Schoelkopf, Strong coupling of a single photon to a superconducting qubit using circuit quantum electrodynamics, *Nature* **431**, 162 (2004).
 - [2] A. Blais, A. L. Grimsmo, S. M. Girvin, and A. Wallraff, Circuit quantum electrodynamics, *Rev. Mod. Phys.* **93**, 025005 (2021).
 - [3] A. Wallraff, D. I. Schuster, A. Blais, L. Frunzio, J. Majer, M. H. Devoret, S. M. Girvin, and R. J. Schoelkopf, Approaching Unit Visibility for Control of a Superconducting Qubit with Dispersive Readout, *Phys. Rev. Lett.* **95**, 060501 (2005).
 - [4] A. Blais, R.-S. Huang, A. Wallraff, S. M. Girvin, R. J. Schoelkopf, and Cavity quantum electrodynamics for superconducting electrical circuits, An architecture for quantum computation, *Phys. Rev. A* **69**, 062320 (2004).
 - [5] F. Arute, K. Arya, R. Babbush, D. Bacon, J. C. Bardin, R. Barends, R. Biswas, S. Boixo, F. G. Brandao, D. A. Buell, and B. Burkett, Quantum supremacy using a programmable superconducting processor, *Nature* **574**, 505 (2019).
 - [6] A. W. Cross, L. S. Bishop, S. Sheldon, P. D. Nation, and J. M. Gambetta, Validating quantum computers using randomized model circuits, *Phys. Rev. A* **100**, 032328 (2019).
 - [7] M. Ruggenthaler, N. Tancogne-Dejean, J. Flick, H. Appel, and A. Rubio, From a quantum-electrodynamical light-matter description to novel spectroscopies, *Nat. Rev. Chem.* **2**, 0118 (2018).
 - [8] Z.-L. Xiang, S. Ashhab, J. Q. You, and F. Nori, Hybrid quantum circuits: Superconducting circuits interacting with other quantum systems, *Rev. Mod. Phys.* **85**, 623 (2013).
 - [9] A. A. Clerk, K. W. Lehnert, P. Bertet, J. R. Petta, and Y. Nakamura, Hybrid quantum systems with circuit quantum electrodynamics, *Nat. Phys.* **16**, 257 (2020).
 - [10] Y. Kubo, F. R. Ong, P. Bertet, D. Vion, V. Jacques, D. Zheng, A. Dréau, J.-F. Roch, A. Auffeves, F. Jelezko, J. Wrachtrup, M. F. Barthe, P. Bergonzo, and D. Esteve, Strong Coupling of a Spin Ensemble to a Superconducting Resonator, *Phys. Rev. Lett* **105**, 140502 (2010).
 - [11] D. I. Schuster, A. P. Sears, E. Ginossar, L. DiCarlo, L. Frunzio, J. J. L. Morton, H. Wu, G. A. D. Briggs, B. B. Buckley, D. D. Awschalom, and R. J. Schoelkopf,

- High-Cooperativity Coupling of Electron-Spin Ensembles to Superconducting Cavities, *Phys. Rev. Lett.* **105**, 140501 (2010).
- [12] R. Amsüss, C. Koller, T. Nöbauer, S. Putz, S. Rotter, K. Sandner, S. Schneider, M. Schramböck, G. Steinhäuser, H. Ritsch, J. Schmiedmayer, and J. Majer, Cavity QED with Magnetically Coupled Collective Spin States, *Phys. Rev. Lett.* **107**, 060502 (2011).
- [13] S. Weichselbaumer, P. Natzkin, C. W. Zollitsch, M. Weiler, R. Gross, and H. Huebl, Quantitative Modeling of Superconducting Planar Resonators for Electron Spin Resonance, *Phys. Rev. Appl.* **12**, 024021 (2019).
- [14] P. Bushev, A. K. Feofanov, H. Rotzinger, I. Protopopov, J. H. Cole, C. M. Wilson, G. Fischer, A. Lukashenko, and A. V. Ustinov, Ultralow-power spectroscopy of a rare-earth spin ensemble using a superconducting resonator, *Phys. Rev. B* **84**, 060501(R) (2011).
- [15] S. Probst, A. Tkalčec, H. Rotzinger, D. Rieger, J.-M. L. Floch, M. Goryachev, M. E. Tobar, A. V. Ustinov, and P. A. Bushev, Three-dimensional cavity quantum electrodynamics with a rare-earth spin ensemble, *Phys. Rev. B* **90**, 100404(R) (2014).
- [16] C. Bonizzoni, A. Ghirri, M. Atzori, L. Sorace, R. Sessoli, and M. Affronte, Coherent coupling between vanadyl phthalocyanine spin ensemble and microwave photons: Towards integration of molecular spin qubits into quantum circuits, *Sci. Rep.* **7**, 13096 (2017).
- [17] M. Mergenthaler, J. Liu, J. J. L. Roy, N. Ares, A. L. Thompson, L. Bogani, F. Luis, S. J. Blundell, T. Lancaster, A. Ardavan, G. A. D. Briggs, P. J. Leek, and E. A. Laird, Strong Coupling of Microwave Photons to Antiferromagnetic Fluctuations in an Organic Magnet, *Phys. Rev. Lett.* **119**, 147701 (2017).
- [18] I. Gimeno, W. Kersten, M. C. Pallarés, P. Hermosilla, M. J. Martínez-Pérez, M. D. Jenkins, A. Angerer, C. Sánchez-Azqueta, D. Zueco, J. Majer, A. Lostao, and F. Luis, Enhanced molecular spin-photon coupling at superconducting nanoconstrictions, *ACS Nano* **14**, 8707 (2020).
- [19] C. Bonizzoni, A. Ghirri, F. Santanni, M. Atzori, L. Sorace, R. Sessoli, and M. Affronte, Storage and retrieval of microwave pulses with molecular spin ensembles, *npj Quantum Inf.* **6**, 68 (2020).
- [20] M. Blencowe, Quantum ram, *Nature* **468**, 44 (2010).
- [21] J. T. Muhonen, J. P. Dehollain, A. Laucht, F. E. Hudson, R. Kalra, T. Sekiguchi, K. M. Itoh, D. N. Jamieson, J. C. McCallum, A. S. Dzurak, and A. Morello, Storing quantum information for 30 seconds in a nanoelectronic device, *Nat. Nanotechnol.* **9**, 986 (2014).
- [22] D. D. Awschalom, L. C. Bassett, A. S. Dzurak, E. L. Hu, and J. R. Petta, Quantum spintronics: Engineering and manipulating atom-like spins in semiconductors, *Science* **339**, 1174 (2013).
- [23] M. D. Jenkins, D. Zueco, O. Roubeau, G. Aromí, J. Majer, and F. Luis, A scalable architecture for quantum computation with molecular nanomagnets, *Dalton Trans.* **45**, 16682 (2016).
- [24] G. Tosi, F. A. Mohiyaddin, V. Schmitt, S. Tenberg, R. Rahman, G. Klimeck, and A. Morello, Silicon quantum processor with robust long-distance qubit couplings, *Nat. Commun.* **8**, 450 (2017).
- [25] S. Carretta, D. Zueco, A. Chiesa, A. Gómez-León, and F. Luis, A perspective on scaling up quantum computation with molecular spins, *Appl. Phys. Lett.* **118**, 240501 (2021).
- [26] B. P. Lanyon, M. Barbieri, M. P. Almeida, J. T. T. C. Ralph, K. J. Resch, G. J. Pryde, J. L. O'Brien, A. Gilchrist, and A. G. White, Simplifying quantum logic using higher-dimensional Hilbert spaces, *Nat. Phys.* **5**, 134 (2008).
- [27] E. T. Campbell, Enhanced Fault-Tolerant Quantum Computing in d -Level Systems, *Phys. Rev. Lett.* **113**, 230501 (2014).
- [28] D. Gottesman, A. Kitaev, and J. Preskill, Encoding a qubit in an oscillator, *Phys. Rev. A* **64**, 012310 (2001).
- [29] S. Pirandola, S. Mancini, S. L. Braunstein, and D. Vitali, Minimal qudit code for a qubit in the phase-damping channel, *Phys. Rev. A* **77**, 032309 (2008).
- [30] A. Chiesa, E. Macaluso, F. Petiziol, S. Wimberger, P. Santini, and S. Carretta, Molecular nanomagnets as qubits with embedded quantum-error correction, *J. Phys. Chem. Lett.* **11**, 8610 (2020).
- [31] F. Tacchino, A. Chiesa, R. Sessoli, I. Tavernelli, and S. Carretta, Molecular spin qudits for quantum simulation of light-matter interactions, submitted (2021).
- [32] A. Gaita-Ariño, F. Luis, S. Hill, and E. Coronado, Molecular spins for quantum computation, *Nat. Chem.* **11**, 301 (2019).
- [33] M. Atzori and R. Sessoli, The second quantum revolution: Role and challenges of molecular chemistry, *J. Am. Chem. Soc.* **141**, 11339 (2019).
- [34] F. Luis, A. Repollés, M. J. Martínez-Pérez, D. Aguilá, O. Roubeau, D. Zueco, P. J. Alonso, M. Evangelisti, A. Camón, J. Sesé, L. A. Barrios, and G. Aromí, Molecular Prototypes for Spin-Based CNOT and SWAP Quantum Gates, *Phys. Rev. Lett.* **107**, 117203 (2011).
- [35] D. Aguilá, D. Barrios, V. Velasco, O. Roubeau, A. Repollés, P. Alonso, J. Sesé, S. Teat, F. Luis, and G. Aromí, Heterodimetallic [LnLn'] lanthanide complexes: Toward a chemical design of two-qubit molecular spin quantum gates, *J. Am. Chem. Soc.* **136**, 14215 (2014).
- [36] J. Ferrando-Soria, E. Moreno-Pineda, A. Chiesa, A. Fernández, S. A. Magee, S. Carretta, P. Santini, I. Vitorica-Yrezabal, F. Tuna, E. J. L. McInness, and R. E. P. Winpenny, A modular design of molecular qubits to implement universal quantum gates, *Nat. Commun.* **7**, 11377 (2016).
- [37] M. D. Jenkins, Y. Duan, B. Diosdado, J. J. García-Ripoll, A. Gaita-Ariño, C. Giménez-Saiz, P. J. Alonso, E. Coronado, and F. Luis, Coherent manipulation of three-qubit states in a molecular single-ion magnet, *Phys. Rev. B* **95**, 064423 (2017).
- [38] E. Moreno-Pineda, M. Damjanović, O. Fuhr, W. Wernsdorfer, M. Ruben, and Nuclear spin isomers, Engineering a $\text{Et}_4\text{N}[\text{DyPc}_2]$ spin qudit, *Angewandte Chemie International Edition* **56**, 9915 (2017).
- [39] E. Moreno-Pineda, C. Godfrin, F. Balestro, W. Wernsdorfer, and M. Ruben, Molecular spin qudits for quantum algorithms, *Chem. Soc. Rev.* **47**, 501 (2018).
- [40] F. Luis, P. J. Alonso, O. Roubeau, V. Velasco, D. Zueco, D. Aguilá, J. I. Martínez, L. A. Barrios, and G. Aromí, A dissymmetric [Gd₂] coordination molecular dimer hosting six addressable spin qubits, *Commun. Chem.* **3**, 176 (2020).

- [41] I. Gimeno, A. Urtizberea, J. Román-Roche, D. Zueco, A. Camón, P. J. Alonso, O. Roubeau, and F. Luis, Broad-band spectroscopy of a vanadyl porphyrin: A model electronuclear spin qudit, *Chem. Sci.* (2021).
- [42] G. Burkard and J. R. Petta, Dispersive readout of valley splittings in cavity-coupled silicon quantum dots, *Phys. Rev. B* **94**, 195305 (2016).
- [43] S. Kohler, Dispersive readout: Universal theory beyond the rotating-wave approximation, *Phys. Rev. A* **98**, 023849 (2018).
- [44] X. Mi, M. Benito, S. Putz, D. M. Zajac, J. M. Taylor, G. Burkard, and J. R. Petta, A coherent spin-photon interface in silicon, *Nature* **555**, 599 (2018).
- [45] L. Pereira, J. García-Ripoll, and T. Ramos, Superradiant phase transition in electronic systems and emergent topological phases (2021), [ArXiv:2109.06616](https://arxiv.org/abs/2109.06616).
- [46] D. Gatteschi, R. Sessoli, and J. Villain, *Molecular Nanomagnets* Vol. 5 (Oxford University Press, New York, 2006).
- [47] J. Bartolomé, F. Luis, and J. F. Fernández, *Molecular Magnets: Physics and Applications* (Springer, Berlin, Heidelberg, 2016).
- [48] A. Muthukrishnan and C. R. Stroud, Multivalued logic gates for quantum computation, *Phys. Rev. A* **62**, 052309 (2000).
- [49] G. K. Brennen, D. P. O’Leary, and S. S. Bullock, Criteria for exact qudit universality, *Phys. Rev. A* **71**, 052318 (2005).
- [50] C. V. Kraus, M. M. Wolf, and J. I. Cirac, Quantum simulations under translational symmetry, *Phys. Rev. A* **75**, 022303 (2007).
- [51] M. D. Jenkins, U. Naether, M. Ciria, J. Sesé, J. Atkinson, C. Sánchez-Azqueta, E. d. Barco, J. Majer, D. Zueco, and F. Luis, Nanoscale constrictions in superconducting coplanar waveguide resonators, *Appl. Phys. Lett.* **105**, 162601 (2014).
- [52] D. Zueco, G. M. Reuther, S. Kohler, and P. Hänggi, Qubit-oscillator dynamics in the dispersive regime: Analytical theory beyond the rotating-wave approximation, *Phys. Rev. A* **80**, 033846 (2009).
- [53] A. Lupascu, S. Saito, T. Picot, P. C. de Groot, C. J. P. M. Harmans, and J. E. Mooij, Quantum non-demolition measurement of a superconducting two-level system, *Nat. Phys.* **3**, 119 (2007).
- [54] T. Nakajima, A. Noiri, J. Yoneda, M. R. Delbecq, P. Stano, T. Otsuka, K. Takeda, S. Amaha, G. Allison, K. Kawasaki, A. Ludwig, A. D. Wieck, D. Loss, and S. Tarucha, Quantum non-demolition measurement of an electron spin qubit, *Nat. Nanotechnol.* **14**, 555 (2019).
- [55] A. Asenjo-García, H. J. Kimble, and D. E. Chang, Optical waveguiding by atomic entanglement in multilevel atom arrays, *Proc. Nat. Acad. Sci.* **116**, 25503 (2019).
- [56] S. G. Ovchinnikov and V. V. Val’kov, *Hubbard Operators in the Theory of Strongly Correlated Electrons* (Imperial College Press, London, 2004).
- [57] C. W. Gardiner and M. J. Collett, Input and output in damped quantum systems: Quantum stochastic differential equations and the master equation, *Phys. Rev. A* **31**, 3761 (1985).
- [58] P. Forn-Díaz, L. Lamata, E. Rico, J. Kono, and E. Solano, Ultrastrong coupling regimes of light-matter interaction, *Rev. Mod. Phys.* **91**, 025005 (2019).
- [59] B. Perez-González, A. Gómez-León, and G. Platero, Topology detection in cavity QED (2021), [ArXiv:2106.08709](https://arxiv.org/abs/2106.08709).
- [60] J. R. Schrieffer and P. A. Wolff, Relation between the Anderson and Kondo Hamiltonians, *Phys. Rev.* **149**, 491 (1966).
- [61] M. W. Doherty, F. Dolde, H. Fedder, F. Jelezko, J. Wrachtrup, N. B. Manson, and L. C. L. Hollenberg, Theory of the ground-state spin of the NV⁻ center in diamond, *Phys. Rev. B* **85**, 205203 (2012).
- [62] S. Putz, D. O. Krimer, R. Amsüss, A. Valookaran, T. Nöbauer, J. Schmiedmayer, S. Rotter, and J. Majer, Protecting a spin ensemble against decoherence in the strong-coupling regime of cavity QED, *Nat. Phys.* **10**, 720 (2014).
- [63] J. van Rantwijk, M. Grim, D. van Loon, S. Yates, A. Baryshev, and J. Baselmans, Multiplexed readout for 1000-pixel arrays of microwave kinetic inductance detectors, *IEEE Trans. Microw. Theory Tech.* **64**, 1876 (2016).
- [64] A. Castro, A. G. Carrizo, S. Roca, D. Zueco, and F. Luis, Optimal Control of Molecular Spin Qudits, *Phys. Rev. Appl.* **17**, 064028 (2022).
- [65] J. M. Zadrozny, J. Niklas, O. G. Poluektov, and D. E. Freedman, Millisecond coherence time in a tunable molecular electronic spin qubit, *ACS Cent. Sci.* **1**, 488 (2015).
- [66] R. Hussain, G. Allodi, A. Chiesa, E. Garlatti, D. Mitcov, A. Konstantatos, K. S. Pedersen, R. De Renzi, S. Piligkos, and S. Carretta, Coherent manipulation of a molecular Ln-based nuclear qudit coupled to an electron qubit, *J. Am. Chem. Soc.* **140**, 9814 (2018). [ArXiv:1909.02374](https://arxiv.org/abs/1909.02374).
- [67] V. Rollano, M. C. de Ory, C. D. Buch, M. Rubín-Osanz, D. Zueco, C. Sánchez-Azqueta, A. Chiesa, D. Granados, S. Carretta, A. Gomez, S. Piligkos, and F. Luis, High cooperativity coupling to nuclear spins on a circuit QED architecture, (2022) [arXiv preprint ArXiv:2203.00965](https://arxiv.org/abs/2203.00965).
- [68] N. V. Prokof’ev and P. C. E. Stamp, Theory of the spin bath, *Rep. Prog. Phys.* **63**, 669 (2000).
- [69] A. Gómez-León, Spin bath dynamics and dynamical renormalization group, *Phys. Rev. B* **100**, 094308 (2019).
- [70] A. Gómez-León, From molecular spins to multi-qudit interactions (2022), [ArXiv:2112.09714](https://arxiv.org/abs/2112.09714).
- [71] C. Bonizzoni, A. Ghirri, S. Nakazawa, S. Nishida, K. Sato, T. Takui, and M. Affronte, Transmission spectroscopy of molecular spin ensembles in the dispersive regime, *Adv. Quantum Technol.* **4**, 2100039 (2021).